Title Page

TAK1 blockade as a therapy for retinal neovascularization

Fan-Li Lin[1,2†], Jiang-Hui Wang[3†], Jinying Chen[2,4], Linxin Zhu[2,4], Yu-Fan Chuang[1,2], Leilei Tu[4], Chenkai Ma[5], Suraj Lama[2], Damien Ling[3], Raymond Ching-Bong Wong[3,6], Alex W. Hewitt[2,3], Ching-Li Tseng[7], Bang V. Bui[8], Peter van Wijngaarden[3,6], Gregory J. Dusting[3,6], Peng-Yuan Wang[1], Guei-Sheung Liu[2,6,9*]

[1]Shenzhen Key Laboratory of Biomimetic Materials and Cellular Immunomodulation, Shenzhen Institute of Advanced Technology, Chinese Academy of Sciences, Shenzhen, China

[2]Menzies Institute for Medical Research, University of Tasmania, Hobart, Australia

[3]Centre for Eye Research Australia, Royal Victorian Eye and Ear Hospital, East Melbourne, Australia

[4]Department of Ophthalmology, the First Affiliated Hospital of Jinan University, Guangzhou, China

[5]Molecular Diagnostics Solutions, CSIRO Health and Biosecurity, North Ryde, New South Wales, Australia

[6]Ophthalmology, Department of Surgery, University of Melbourne, East Melbourne, Victoria, Australia

[7]Graduate Institute of Biomedical Materials and Tissue Engineering, College of Biomedical Engineering, Taipei Medical University, Taipei, Taiwan

[8]Department of Optometry and Vision Sciences, University of Melbourne, Parkville, Victoria, Australia

[9]Aier Eye Institute, Changsha, Hunan, China

†FLL and JHW contributed equally to this work.

*Correspondence and requests for materials should be addressed to Dr Guei-Sheung Liu (rickliu0817@gmail.com). Menzies Institute for Medical Research, University of Tasmania. Address: 17 Liverpool Street, Hobart, TAS 7000, Australia. Tel: +61362264250.

Running title: Targeting TAK1 alleviates retinal neovascularization

Key words: TAK1, inflammation, angiogenesis, retinal neovascularization, oxygen-induced retinopathy

ABSTRACT

Retinal neovascularization, or pathological angiogenesis in the retina, is a leading cause of blindness in developed countries. Transforming growth factor-β-activated kinase 1 (TAK1) is a mitogen-activated protein kinase kinase kinase (MAPKKK) activated by TGF-β1 and other pro-inflammatory cytokines. TAK1 is also a key mediator of inflammation, innate immune responses, apoptosis and tissue homeostasis and plays an important role in physiological angiogenesis. Its role in pathological angiogenesis, particularly in retinal neovascularization, remains unclear. We investigated the regulatory role of TAK1 in pathological angiogenesis in the retina. Transcriptome analysis of human retina featuring retinal neovascularization revealed enrichment of known TAK1-mediated signaling pathways. Selective inhibition of TAK1 activation by 5Z-7-oxozeaenol attenuated aberrant retinal angiogenesis in rats following oxygen-induced retinopathy. Transcriptome profiling revealed that TAK1 activation in human microvascular endothelial cells under TNFα stimulation led to increase the gene expression related to cytokines and leukocyte-endothelial interaction, mainly through nuclear factor kappa B (NFκB) signaling pathways. These results reveal that inhibition of TAK1 signaling may have therapeutic value for the treatment of pathological angiogenesis in the retina.

INTRODUCTION

Retinal neovascularization is a severe complication of several ocular diseases, often resulting in permanent damage to the neurosensory retina and irreversible vision loss (1). Retinal neovascularization shares similar characteristics to pathological angiogenesis elsewhere in the body, exhibiting features including endothelial proliferation and migration, elevated vascular permeability and inflammation; all processes in which vascular endothelial growth factor (VEGF) plays a crucial role (2). Recently, the advent of ocular anti-VEGF therapies has been a significant advance in mitigating the risk of vison loss associated with retinal neovascularization. Despite this success, there is increasing evidence that some patients do not respond well to anti-VEGF treatments (3). Therefore, it is necessary to seek other therapeutic targets.

The common pathways shared between inflammation and angiogenesis play critical roles in retinal neovascularization (4). Several studies have reported increased expression of various pro-inflammatory cytokines, chemokines, pro-angiogenic factors and adhesion molecules in patients with retinal neovascularization, such as tumor necrosis factor α (TNFα), interleukin-1 (IL-1), chemokine (C-X-C motif) ligand 8 (CXCL8; known as IL-8), vascular endothelial growth factor (VEGF), as well as intercellular adhesion molecule 1 (ICAM-1 and VCAM-1) (5-9). TNFα was found to suppress the expression of tight junction proteins and is required for VEGF-mediated hyperpermeability in endothelial cells and the breakdown of the blood-retinal barrier in patients with diabetic retinopathy (DR) (10, 11). Interleukins are also primary mediators of inflammation that can promote angiogenesis via induction of proangiogenic factors such as VEGF (4). Moreover, TNFα and IL-1 stimulates expression of ICAM-1, CXCL8 and VEGF in endothelial cells and microglia cells, both of which promote progression of retinal neovascularization (12, 13). A key role for inflammatory mediators is highlighted by their growing use as prognostic markers of the severity of proliferative diabetic retinopathy (PDR) (4).

Transforming growth factor-β-activated kinase 1 (TAK1), a member of the mitogen-activated protein kinase (MAPK) family, is a critical serine/threonine kinase in several cellular signaling pathways. Such pathways can be activated by diverse pro-inflammatory stimuli including TNFα, IL-1, transforming growth factor beta (TGF-β), or toll-like receptor (TLR) ligands. The engagement of TAK1 in turn activates downstream signaling pathways, including nuclear factor kappa B (NFκB) and MAPK p38, extracellular signal-regulated kinase (ERK), and c-Jun kinase (JNK) signaling, modulating inflammatory responses and cell survival (14-16). TAK1 inhibition has been shown to reduce TNFα and CXCL8 secretion in leukocytes (17) and to suppress prostaglandin-endoperoxide synthase 2 (PTGS2; known as cyclooxygenase-2, COX-2), ICAM-1, and VEGF expression in cancer cells through NFκB signaling pathway (18). Expression of TAK1 provides protection for endothelial

84 cells against TNFα-induced apoptosis under inflammatory conditions (19). Indeed, TAK1 deletion
85 causes embryonic lethality as the capacity to prevent TNFα-induced endothelial cell death and vessel
86 regression is lost. Moreover, TAK1 is also important for supporting TNFα-independent vascular
87 formation and endothelial migration. These broad roles for TAK1 suggests that endothelial TAK1
88 inhibition may be a useful alternate anti-angiogenesis target in retinal disease (19, 20).
89 We hypothesized that TAK1 plays a crucial role in pathological angiogenesis and TAK1 inhibition
90 can suppress retinal neovascularization. Our findings indicate that TAK1 is an important regulator of
91 inflammatory and angiogenesis-related pathways that contribute to retinal neovascularization.
92 Pharmacological inhibition of TAK1 alleviated aberrant retinal angiogenesis by modulating cytokine
93 signaling and leukocyte-endothelium interactions in a rat model of ischemia-induced retinopathy.
94
95
96 **RESULTS**
97 **TAK1 is expressed in human retina and is positively associated with retinal neovascularization**
98 To understand TAK1 expression profiles in the human retina, we first analyzed published single nuclei
99 RNAseq (snRNAseq, GSE135133) data to examine TAK1 expression in different retinal cells.
100 Analysis of 121,799 individual cells from human retina revealed that both *TAK1* (*MAP3K7*) and its
101 binding protein, *TAB1-3,* are expressed moderately in most neural and non-neural retinal cells (**Fig.
102 1A and S1**). Notably, among the retinal cells examined, TAK1 is highly enriched in endothelial cells.
103 Immunostaining suggests that TAK1 is expressed in various layers of the human retina in both neural
104 and non-neural cells, such as mural cells and smooth muscle cells (**Fig. 1B**) in larger vessels (diameter
105 of artery or vein ranging from 0.6 - 16 mm) (21). We also found that co-localization of TAK1 and
106 endothelial cell marker CD31 was more likely to be found in the microvasculature, including arterioles
107 or venules (20 - 25 μm) and capillaries (9 μm).
108 To identify the key molecular signaling or biological pathways relevant to the angiogenic process
109 in patients with retinal neovascularization, a transcriptome dataset from humans with proliferative
110 diabetic retinopathy (PDR) was interrogated by taking advantage of Gene Set Enrichment Analysis
111 (GSEA), a knowledge-based approach for interpreting genome-wide expression profiles (22).
112 Compared with controls, those with retinal neovascularization showed enrichment of known TAK1
113 upstream signaling pathways, including IL1, TNF, TGF-β, TLR, T-cell receptor (TCR) and B-cell
114 receptor (BCR) (**Fig. 1C and S2**). Pathways related directly to TAK1 were enriched, such as "TAK1
115 activation of NFκB by phosphorylation and activation of inhibitor of κB (IκB) kinase (IKK) complex",
116 "activated TAK1 mediated p38 MAPK activation", and "JNK kinases phosphorylation and activation

117 mediated by activated TAK1" (**Fig. 1C and 1D**). In general, genes in association with TAK1 activation
118 mediated by NFκB and MAPKs phosphorylation were up-regulated in patients with retinal
119 neovascularization compared with controls (**Fig. S3**). There was negative enrichment of genes
120 associated with several biological pathways in relation to visual phototransduction and neuronal
121 systems (**Fig 1C**).
122

123 **TAK1 is up-regulated in neovascular tufts and positively associated with retinal**
124 **neovascularization in ischemia-induced retinopathy in rat**

125 To investigate the role of TAK1 in pathological neovascularization in the retina, we subsequently used
126 a rat model of oxygen-induced retinopathy (OIR) which yields ischemic avascular zones and preretinal
127 neovascularization similar to that observed clinically in PDR and retinopathy of prematurity. Neonatal
128 rats were subjected to daily cycles of 80% oxygen for 21 hours and ambient air for 3 hours from
129 postnatal day 0 (P0) to P14 to induce vaso-obliteration. At P14 rats were returned to room air, where
130 maximal preretinal neovascularization occurred by P18, which was followed by a phase of vascular
131 regression (**Fig. 2A**). A significant increase in TAK1 expression at both RNA and protein levels was
132 observed in OIR retinae at P18 compared with controls (**Fig. 2B and 2C**). Examination of the retinal
133 distribution of TAK1 expression revealed that TAK1 expression was uniquely expressed in areas of
134 active neovascularization (**Fig. 2D**). To gain further insight into the role of TAK1 activation at the
135 peak of retinal neovascularization (P18), we then performed transcriptome analyses using bulk-RNA
136 sequencing. GSEA-based analysis revealed a positive enrichment of several TAK1 upstream pathways,
137 including IL1, TNF, TCR, BCR and TLR (**Fig. 2E and S4**), which is consistent with our findings in
138 patients with retinal neovascularization due to PDR. Similar to findings in humans, there was a
139 negative enrichment of genes associated with phototransduction and neuronal systems at P18 in the
140 rats. Of note, certain canonical pathways and biological processes related to angiogenesis were
141 positively enriched in the OIR model, such as VEGF-A/VEGFR2, PDGF pathway, the cellular
142 response to hypoxia, angiogenesis and inflammation (**Fig. 2E and S4**). Overall, our data implicates
143 active involvement of TAK1 in retinal neovascularization.
144

145 **Inhibition of TAK1 activation attenuates retinal neovascularization in rat OIR model**

146 Given that the ablation of TAK1 in endothelial cells impairs angiogenesis and causes lethality (19, 20),
147 we therefore used a selective inhibitor of TAK1, 5Z-7-oxozeaenol, a resorcylic acid lactone derived
148 from a fungus (23), to assess whether TAK1 signaling blockade can alleviate retinal neovascularization.
149 5Z-7-oxozeaenol was administered intravitreally to the OIR rats at P14 (**Fig. 3A**). Four days after drug

150 administration, retinal neovascularization was significantly suppressed by 51.3% and 57.1% in OIR
151 rats that had received low (18 ng) and high doses (90 ng) of 5Z-7-oxozeaenol, respectively, compared
152 to OIR rats that had vehicle only (**Fig. 3B and S5**). No significant difference in retinal vaso-obliteration
153 was found among these groups (**Fig. 3C**). We also examined the development of deep capillary beds
154 to assess the effects of TAK1 inhibition in physiological vessel growth (24). Normal control rats
155 developed a complete deep layer vasculature, while such development was severely disrupted in OIR
156 rats (**Fig. 3D**). We found that 5Z-7-oxozeaenol treatment did not improve or damage the formation of
157 deep capillary beds in OIR retina, which is likely attributed to suppression of proliferative vessels by
158 TAK1 inhibition. Moreover, the rats receiving low or high dose of 5Z-7-oxozeaenol did not show any
159 abnormalities in the retinal vasculature under normoxic conditions (**Fig. S6**).
160

161 **TAK1 deletion impairs the expression of multiple cytokines and cell adhesion molecules in**
162 **endothelial cells responding to inflammatory insults**

163 Given that TAK1 blockade prevented retinal neovascularization and previous studies have indicated
164 that TAK1 is activated in response to various pro-inflammatory stimuli such as TNFα, IL-1β, TGF-β,
165 or TLR ligand, we evaluated what signaling regulates TAK1 in the endothelial response to
166 inflammation. We first generated TAK1-knockout (KO) human telomerase-immortalized
167 microvascular endothelial (TIME) cells (TAK1-KO) using CRISPR/Cas9 (**Fig. S7**). To explore the
168 effect of TAK1 deletion in human microvascular endothelial cells, we generated a transcriptome
169 profile through bulk-RNA sequencing of wild-ype TIME cells (WT) and TAK1-KO TIME cells
170 (TAK1-KO). We found that 2178 genes (743 upregulation and 1435 downregulation) were
171 differentially expressed [false discovery rate (FDR), <0.05] following TAK1-KO (**Fig. S8A and S8B**).
172 GSEA results suggested that TAK1 knockout negatively affected pathways related to tissue immune
173 responses, cell adhesion, and cell-extracellular matrix interaction (**Fig. S8C**).

174 Since TNFα is strongly correlated with progression of retinal neovascularization and is a major
175 activator of TAK1 signaling (10), we performed bulk-RNA sequencing to obtain transcriptomes from
176 wild-type (WT) TIME cells and TAK1-KO TIME cells that were in the presence or absence of TNFα
177 (**Fig. 4A**). We found that 462 and 3609 genes were differentially expressed (FDR<0.05 and
178 Log2FoldChange >1 or <-1) in wild-type cells upon TNFα treatment (WT TNF *vs.* WT; hereafter
179 referred to as the WT TNF set) and TAK1-KO cells upon TNFα treatment (TAK1-KO TNF *vs.* WT
180 TNF; hereafter referred to as the TAK1-KO TNF set), respectively (**Fig. 4B**). To further explore the
181 biological significance of our findings in differential gene expression, we undertook GSEA of WT
182 TNF and TAK1-KO TNF sets. GSEA results showed the top 20 KEGG (Kyoto Encyclopedia of Genes
183 and Genomes) gene sets were positively enriched due to TNFα stimulation in WT cells (**Fig. 4C**).

184 However, in TAK1-KO cells exposed to TNFα, 7 of the top 10 gene sets were negatively enriched,
185 suggesting that these biological functions (highlighted in red in **Fig.4C**) induced by TNFα were
186 adversely affected in cells due to TAK1 knockout. The gene sets related to cytokines ("Cytokine-
187 cytokine receptor interaction") and cell adhesion molecules ("Cell adhesion molecules-CAM") were
188 positively enriched in the wild-type cells exposed to TNFα yet not in TAK1-KO cells exposed to TNFα
189 (**Fig. 4C**), indicating the expression of cytokines and cell adhesion molecules induced by TNFα were
190 negatively affected in human microvascular endothelial cells due to TAK1 knockout. We further
191 analyzed the target genes of TAK1 in these two gene sets by a Venn diagram. A total of 74 cytokine-
192 related genes and 29 cell adhesion molecule-related genes were positively enriched in TNFα-treated
193 WT cells (**Fig. 4D and 4E**). Among of these genes, 59 cytokine-related genes and 23 cell adhesion
194 molecule-related genes were negatively enriched in TNFα-treated TAK1-KO cells (**Fig. 4D and 4E**).
195 Many of these genes are related to inflammation and angiogenesis, suggesting that TAK1 may be
196 involved in the regulation of the production of proinflammatory/proangiogenic cytokines (such as
197 *CXCL8* and *VEGFA*), as well as leukocyte-endothelial interactions (leukostasis; such as *ICAM-1* and
198 *VCAM-1*) in retinal neovascularization (**Fig. 4F**).
199
200 **TAK1 is required for activation of NFκB signaling in mediating the expression of multiple**
201 **cytokines and cell adhesion molecules in endothelial cells responding to inflammatory insults**
202 NFκB and MAPKs signaling are the primary known downstream pathways mediated by TAK1
203 activation, both of which have been shown as key mediators involved in several pathological
204 conditions associated to angiogenesis, such as arthritis and cancer (25, 26) (**Fig. 5A**). We therefore
205 investigated whether the identified 59 cytokine-related genes and 23 cell adhesion molecule-related
206 genes from TNFα-treated TAK1-KO cells are regulated by NFκB and MAPKs signaling pathway. We
207 found that about 75% (38/59) of selected genes from the "cytokine gene set" and 35% (8/23) of
208 selected genes from the "adhesion molecule gene set" are known to be regulated by NFκB and activator
209 protein-1 (AP-1, a transcription factor regulates by MAPK signaling cascade), both of which were
210 identified from a NFκB target gene database (27) and ENCODE Transcription Factor Targets Database,
211 respectively (**Fig 5B and Table 1**).
212 To confirm the impairment of the activation of NFκB and MAPKs signaling caused by TAK1
213 knockout, we characterized the activation of NFκB and MAPKs in TNFα-treated TAK1-KO cells.
214 TNFα treatment significantly increased TAK1 phosphorylation in WT cells, an effect not observed in
215 TAK1-KO cells (**Fig. 5C and 5D**). IκB degradation and NFκB p65 phosphorylation are key events in
216 NFκB signaling (28). TNFα treatment significantly induced NFκB p65 phosphorylation and IκB

217 degradation in WT cells, while no such changes occurred in TAK1-KO cells (**Fig. 5C and 5E**).
218 Likewise, phosphorylation of JNK, p38, and ERK in MAPK signaling was not increased in TNFα-
219 treated TAK1-KO cells compared to TNFα-treated wild-type cells (**Fig. 5C and 5F**). Collectively,
220 these data indicate that TAK1 is required for phosphorylation of the key mediators of NFκB and
221 MAPK signaling in human microvascular endothelial cells.
222 Expression of the most significant genes (those also shown to be involved in retinal
223 neovascularization) from the gene sets related to cytokines ("Cytokine-cytokine receptor interaction")
224 and cell adhesion molecules ("Cell adhesion molecules-CAM") was also validated using qRT-PCR.
225 Upon TNFα stimulation, the expression level of *CXCL8*, *VEGF-A, ICAM-1*, and *VCAM-1*, were
226 substantially elevated in WT cells, while no TNFα induced change was observed in TAK1-KO cells
227 (**Fig. 5G**). Similar results were found in IL1β-treated WT cells but not in IL1β-treated TAK1-KO cells
228 (**Fig. S9**). Likewise, TAK1 knockdown using TAK1 siRNA (siTAK1) or TAK1 inhibitor (5Z-7-
229 oxozeaenol) resulted in a similar effect in primary human retinal microvascular endothelial cells
230 (HRMECs) (**Fig. S10 and S11**). These data further confirmed that TAK1 is required for activation of
231 NFκB/AMPKs signaling to regulate expression of multiple cytokines and cell adhesion molecules in
232 human microvascular endothelial cells responding to inflammation.
233
234 **Pharmacological inhibition of TAK1 suppresses the expression of inflammatory cytokines and**
235 **reduces leukocyte-endothelial interactions (leukostasis) in the rat OIR model, while has no**
236 **impact on retinal structure and function**
237 To further confirm the effect of TAK1 inhibition in suppressing the expression of inflammatory
238 cytokines and reduces leukostasis in the development of retinal neovascularization, OIR rats were
239 treated with 5Z-7-oxozeaenol at P14 and the retinae were harvested for qPCR and histological analysis
240 at the time points indicated in the figure (**Fig. 6A**). Two days after drug administration, TAK1
241 inhibition attenuated the expression of inflammatory and angiogenic genes, including *TNFα*, *VEGFA*
242 and *ICAM-1*, in the retina of OIR rats that had received low (18 ng) and high doses (90 ng) of 5Z-7-
243 oxozeaenol, respectively, compared to OIR rats that had vehicle only, suggesting that 5Z-7-oxozeaenol
244 can mitigate the production of inflammatory and angiogenic cytokines in the progression of retinal
245 neovascularization (**Fig. 6B**). Since TAK1 was found to modulate the expression of cell adhesion
246 molecules in human endothelial cells responding to proinflammatory cytokine, we therefore further
247 evaluated the event of microglial adhesion to the vascular surface (leukostasis). Co-immunostaining
248 of isolectin GS-IB4 (blood vessel) and Iba1 (a marker of microglia) illustrated that 5Z-7-oxozeaenol
249 treatment at both low and high doses significantly attenuated the microglial adhesion to the vascular

250 surface in OIR rats (**Fig. 6C and 6D**). Together, our data suggest that active involvement of TAK1 in
251 the regulation of proinflammatory and proangiogenic cytokine expression as well as modulation of
252 leukostasis in the retinal vasculature. Thus, 5Z-7-oxozeaenol is therapeutically effective to suppress
253 retinal neovascularization in the rat model of retinopathy (**Fig. 6E**).

254 In addition to examining the therapeutic efficacy of 5Z-7-oxozeaenol in retinal neovascularization,
255 we further performed safety evaluations to test whether 5Z-7-oxozeaenol adversely affects rodent
256 retinae. Electroretinography (ERG) and optical coherence tomography (OCT) were performed to look
257 for any retinal functional or structural changes in rats 28 days post intravitreal injection of high dose
258 of 5Z-7-oxozeaenol. No difference in function was observed for photoreceptors, bipolar cells or
259 ganglion cells between vehicle- or 5Z-7-oxozeaenol-treated eyes (**Fig. S13A-S13F**). No significant
260 difference was observed in total retinal thickness or thickness of various retinal layers including the
261 nerve fiber layer (NFL) and outer retina layer (ORL) between 5Z-7-oxozeaenol- and vehicle-treated
262 eyes (**Fig. S13G and S13H**). Together, these results suggested that intravitreal injection of 5Z-7-
263 oxozeaenol does not result in adverse or toxic effects on retinal function and structure up to 28 days
264 post-injection.

265

266

267 **DISCUSSION**

268 TAK1 is a key modulator involved in a range of cellular functions including the immune response (14),
269 cell survival and death (16), angiogenesis (20), fibrosis (29) and tumor metastasis (30). TAK1 is
270 activated in response to various stimuli such as pro-inflammatory cytokines, hypoxia, oxidative stress,
271 metabolism, DNA damage, Wnt and osmotic shock (14, 31-33). Whether TAK1 is involved in
272 angiogenesis or inflammatory signaling in the retina, much less the molecular mechanisms by which
273 this occurs, has not been studied. Here, we show that TAK1 plays a central role in regulating
274 inflammatory and angiogenic signaling in the rat retina, and that the same signaling appears to be
275 involved in human diabetic retinopathy. Pharmacological antagonism of TAK1 signaling by 5Z-7-
276 oxozeaenol was shown to be a potential therapeutic option for retinal neovascularization.

277 NFκB and MAPK are critical regulators of stress responses, immunity, inflammation and
278 angiogenesis. A variety of proinflammatory cytokines such as TNFα and IL1β activate these signaling
279 pathways through a common upstream kinase TAK1 (34). For instance, TNFα binds to its receptor 1
280 (TNFR1) upon inflammatory stimuli, triggering TAK1 that in complex with TAB1-3 phosphorylate
281 IKK at Ser^{177} and Ser^{181}, which in turn leads to rapid proteasome-mediated degradation of the IκB
282 subunit. Subsequently, NFκB (p50/p65) is activated and translocated to the nucleus to promote gene

transcription (17). In addition, the TAK1 complex phosphorylates MAPKs to activate the JNK pathway and the p38 MAPK pathways (both mediated by MKK4 and MKK7) as well as ERK by an IKK2/tumor progression locus 2 (TPL2)-dependent pathway (35). Phosphorylation of p38 affects F-actin polymerization in vascular endothelial cells and endothelial migration (36). Activation of JNK and ERK subsequent to p21-activated kinase 1 stimulation promotes endothelial migration through enhancement of cell motility (37). In particular, ERK is involved in VEGF-induced endothelial proliferation, migration (via actin polymerization, lamellipodia and filopodia formation and myosin contraction), morphogenesis (tube formation) and extracellular matrix degradation during angiogenesis (37). In fact, deletion of TAK1 leads to the inactivation of both JNK and NFκB signaling, as well as downregulation of expression of pro-survival genes in mice (38). Hence, deletion of TAK1 causes bone marrow and liver failure in mice due to the massive apoptotic death of hematopoietic cells and hepatocytes, ultimately resulting in death within a few days. Moreover, endothelial-specific TAK1 knockout mice demonstrated intestinal and liver hemorrhage secondary to apoptosis of endothelial cells and damaged vessels, resulting in rapid death (19). These data suggest that TAK1 protects endothelial cells and maintains vascular integrity and homeostasis under inflammatory conditions.

Here, we provide the first evidence that both genetic and pharmacological inhibition of TAK1 activity in human microvascular endothelial cells prevents inflammatory stimuli from inducing sequential phosphorylation of upstream kinases in both NFκB (p65) and MAPKs (JNK, p38 and ERK) pathways and suppressed expression of downstream genes that drive inflammation and angiogenesis. GSEA results confirmed that TAK1 knockout prevented TNFα induced cytokines and cell adhesion molecules expression predominantly through the NFκB pathway, resulting in attenuated inflammation and angiogenesis. In addition, TAK1 inhibition by 5Z-7-oxozeaenol in OIR rat significantly reduced cytokines expression and adhesion of microglia to retinal endothelial cells. These data together suggest a significant role for TAK1 in mediating crosstalk between inflammatory and angiogenic pathways, both of which are crucial in pathological angiogenesis.

TAK1 is thus a central regulator of cell survival and death (16). 5Z-7-oxozeaenol, a resorcylic acid lactone derived from a fungus, acts as a potent and selective inhibitor of TAK1, which displays more than 33- and 62-fold selectivity for TAK1 over binding of MEKK1 and MEKK4, respectively (23). It forms a covalent complex with TAK1 and impedes both the kinase and ATPase activity of TAK1 following bi-phase kinetics (39). We demonstrated that intravitreal injection of 5Z-7-oxozeaenol suppressed retinal neovascularization, and modulated elevated TNFα expression in the retina of OIR rats, without causing degeneration of the normal vasculature. These data suggest that TAK1 inhibition by 5Z-7-oxozeaenol may more specifically attenuate active angiogenesis with less risk of damage to normal endothelial cells. However, further studies are required to understand the

317 effects of repeated 5Z-7-oxozeaenol treatment. Moreover, TAK1 Inhibition by 5Z-7-oxozeaenol is
318 known to block pro-inflammatory signaling by selectively inhibiting TAK1 MAPKKK (23). In an
319 animal model of early brain injury, 5Z-7-oxozeaenol was shown to inhibit subarachnoid hemorrhage-
320 induced phosphorylation of p38 and JNK, the nuclear translocation of NFκB p65 and degradation of
321 IκB, ultimately reducing neuronal apoptosis and early brain injury (40). Similarly, another study
322 demonstrated that 5Z-7-oxozeaenol alleviated experimental autoimmune encephalomyelitis by
323 reducing the levels of pro-inflammatory cytokines in splenocytes and the central nervous system, thus
324 reducing the number of activated microglia and blocking p38 MAPK, JNK, and ERK signaling
325 pathways (41). Overactive microglia can damage surrounding cells, via a range of detrimental effects
326 including release of pro-inflammatory cytokines, reactive nitrogen species, reactive oxygen, and
327 proteolytic enzymes (42). We also observed diminished adhesion of microglia to endothelial cells in
328 OIR rats receiving 5Z-7-oxozeaenol treatment, suggesting that 5Z-7-oxozeaenol alleviates
329 inflammation in the retina, in part by reducing activation of microglia. Altogether, our results indicate
330 that TAK1 inhibition by 5Z-7-oxozeaenol suppresses ocular inflammation and neovascularization by
331 inhibiting cellular proliferation and microglia activation through NFκB pathway.

332 5Z-7-oxozeaenol has been previously examined in a number of animal studies focusing on brain
333 injury (43-45). One study demonstrated that 5Z-7-oxozeaenol has neuroprotective function in a mouse
334 model of stroke (43). However, others suggest long-term TAK1 inhibition may not be protective in
335 neurodegenerative disorders (46). Chronic TAK1 inhibition resulted in apoptosis of a number of
336 normal cells, including keratinocytes, hepatocytes, and hematopoietic cells, raising safety concerns
337 (38, 47, 48). We demonstrated that TAK1 inhibition was capable of simultaneously reducing
338 proinflammatory cytokines and proangiogenic cytokines in the retina of OIR rats. In our studies, no
339 adverse effects of intravitreal injection of the TAK1 inhibitor on retinal function or structure were
340 apparent up to 28 days post-injection. Specifically, TAK1 inhibition by intravitreal injection of 5Z-7-
341 oxozeaenol did not affect the scotopic threshold response, a highly sensitive electroretinography
342 measure of retinal ganglion cell activity (49). Another study has shown that systemic TAK1 inhibition
343 by 5Z-7-oxozeaenol preserved β cell function, thus improving overall health condition in the animal
344 with autoimmune diabetes (50). It is worth noting that 5Z-7-oxozeaenol may have off-target effects,
345 potentially stemming from cross-reactivity with other human kinases that possess an analogous
346 cysteine (51). Whilst encouraging, further studies with chronic dosing of 5Z-7-oxozeaenol are clearly
347 needed to confirm safety.

348 In summary, the present study identifies TAK1 as a mediator of inflammatory and angiogenic
349 signaling pathways, with a central role in retinal neovascularization. We demonstrated elevated TAK1
350 signaling in both human and rat retinae associated with neovascularization. We showed that reducing

TAK1 suppressed the expression of multiple cytokines and leukostasis in endothelial cells responding to inflammatory insults *in vitro* through NFκB signaling pathway. Using 5Z-7-oxozeaenol, a well-studied selective TAK1 inhibitor, we demonstrated that pharmacological inhibition of TAK1 can effectively suppress retinal neovascularization in *in vivo* models in rats. These findings provide new insights into the molecular and cellular mechanisms by which TAK1 modulates pathological angiogenesis, thus highlighting a potential alternative approach to anti-VEGF treatment to prevent retinal neovascularization.

361 **MATERIALS AND METHODS**

362 **Data accession**

363 To assess TAK1 expression in human retinal cells, we utilized data single cell transcriptomes from
364 human retina, from the Gene Expression Omnibus
365 (https://www.ncbi.nlm.nih.gov/geo/query/acc.cgi?acc=GSE135133) (accessed on September 20,
366 2020).

367 To access gene expression in retinas from patients with retinal neovascularization due to
368 proliferative diabetic retinopathy, we obtained the RNA-seq raw counts and TPM matrices from the
369 Gene Expression Omnibus (https://www.ncbi.nlm.nih.gov/geo/query/acc.cgi?acc=GSE102485)
370 (accessed on September 27, 2020). We specifically compared samples from patients with retinal
371 neovascular proliferative membranes due to type II diabetes (GSM2739349, GSM2739350 and
372 GSM2739351) and those from normal controls (GSM2739364, GSM2739365 and GSM2739366).

373

374 **scRNA-seq data analysis**

375 scRNA-seq data were retrieved from a public dataset (GSE135133) and analyzed in R (v3.6.3) using
376 Seurat (v3.2) (52, 53) with customized scripts. In brief, cell identity was assigned according to the
377 assignment labels kindly provided by the authors after we normalized and scaled all human samples.
378 We assigned ganglion cells, horizontal cells, bipolar cells, amacrine cells, cones and rods as the neural
379 cells while immune cells, basal cells, red cells, pericytes, endothelial cells, astrocytes and Müller cells
380 were regarded as non-neural cells. Dot plots were utilized for visualization of gene expression levels
381 and percentage difference for various cell types.

382

383 **RNA isolation**

384 Total cells or tissue RNA was isolated using Zymo Quick-RNA MiniPrep kit (R1055; Zymo Research,
385 Irvine, CA) according to the manufacturer's instructions. The quantity of RNA was evaluated with a
386 NanoDrop ND-1000 spectrophotometer (NanoDrop Technologies, Wilmington, DE).

387

388 **RNA-seq analysis**

389 Analysis was undertaken in triplicate on total RNAs (1 μg) from normoxic and OIR rats at P14,
390 prepared as per the manufacturers' instructions. cDNA libraries were sequenced by using an Illumina
391 Hiseq-2500 RNA-seq platform as 50 bp single end chemistry at the Australian Genome Research
392 Facility (AGRF, Melbourne, VIC, Australia). The raw fastq files of single-end reads were removed
393 the adapter sequences and the low-quality reads were dropped by Trimgalore 0.4.4 (Babraham

394 Bioinformatics). Filtering parameter were set as follow: -q 25 --length 50 -e 0.1 --stringency 5. The
395 trimmed reads were subjected to alignment with default setting using STAR 2.5.3. The reference
396 genomes for human and rat were hg38 and rn6, respectively. Aligned RNA-seq data was counted over
397 gene exon using feature Counts (subread 1.6.4). Genes were annotated as per the Gencode Version 33
398 annotation file.
399
400 **Gene set enrichment analysis (GSEA)**
401 GSEA was run on the human dataset of protein-coding genes in PDR versus controls and on the rodent
402 dataset of protein-coding genes in OIR versus controls, against canonical pathway genesets collection
403 (c2.cp.v7.2, Broad Institute) by using 1000 genesets permutations. Only genesets with FDR < 0.05
404 were considered. Readcount values were loaded into R (v3.6.3) for statistical analysis and the heatmap
405 function was used to perform hierarchical clustering analysis and for data representation.
406
407 **Quantitative polymerase chain reaction (qPCR)**
408 Total RNAs (100 ng) was reverse transcribed to cDNA using a High-Capacity cDNA Reverse
409 Transcription kit (4368814; Life Technologies, Carlsbad, CA). Quantitative PCR was performed using
410 TaqMan fast advanced master mix (4444553; Applied Biosystems, Foster City, CA) and gene TaqMan
411 probe sets to detect gene expression (**Table S2**). The expression levels of target genes were normalized
412 to the levels of rat beta-actin (Rn00821065_g1) or human GAPDH (Hs99999905_m1). Subsequently,
413 the ΔΔCt method was used to evaluate relative expression level (fold change) in each condition versus
414 the corresponding control condition.
415
416 **Cell culture**
417 Telomerase-immortalized human microvascular endothelial cell (TIME; CRL-4025™) and primary
418 human retinal microvascular endothelial cell (HRMEC; ACBRI 181V) were purchased from American
419 Type Culture Collection (ATCC; Manassas, VA) and Cell Systems (Kirkland, WA). Endothelial cells
420 were cultured in EBM™ Plus Basal Medium supplied with EGM™ Plus SingleQuots™ supplements
421 (CC-5035; Lonza, Basel, Switzerland). All cell lines were maintained in a humidified incubator at
422 37°C and 5% CO_2. Cell lines were mycoplasma free tested by MycoAlert™ Mycoplasma Detection
423 Kit (LT07; Lonza).
424
425 **Western blotting**
426 A standard immunoblotting protocol was used. Briefly, protein was extracted from cells or retinas with
427 Pierce RIPA buffer (89900; Life Technologies) supplied with protease inhibitor cocktail

428 (11697498001; Roche Diagnostics, Basel, Switzerland). Equal amounts of cell lysates from different
429 groups were subjected to Western blotting analysis with specific antibodies against IκB, phospho-
430 NFκB p65, NFκB p65, phospho-p44/42 MAPK (Erk1/2), p44/42 MAPK (Erk1/2), phospho-TAK1,
431 TAK1, phospho-SAPK/JNK, SAPK/JNK, phospho-p38 MAPK, p38 MAPK (4814, 3033, 4764, 9101,
432 4695, 9339, 4505, 9255, 9252, 9211, 8690, respectively; Cell Signaling), and β-actin (MAB1501;
433 Merck Millipore, Burlington, MA). The quantitative densitometry was analyzed using Image Pro Plus
434 software (Media Cybernetics, Rockville, MA).
435
436 **Animals**
437 Pregnant Sprague-Dawley rats (female, 12-14 weeks old) and Brown Norway rats (male, 12 weeks
438 old) were supplied by the Animal Resources Centre (Murdoch, WA, Australia) and Cambridge Farm
439 Facility of the University of Tasmania (Cambridge, TAS, Australia). Animals were housed in standard
440 cages with a temperature/humidity-controlled and a 12-hour light (50 lux illumination)/12-hour dark
441 (<10 lux illumination) cycle environment. Food and water were available *ad libitum*. All animal
442 experiments were conducted in accordance with guidelines of the ARVO Statement for the Use of
443 Animals in Ophthalmic and Vision Research and were approved by the Animal Ethics Committees of
444 St Vincent's Hospital (004/16), the University of Melbourne (13-044UM), and the University of
445 Tasmania (A0017311). Rats were randomly allocated to treatment groups such that littermates were
446 distributed equally between groups.
447
448 **Rat model of oxygen-induced retinopathy and intravitreal injection of 5Z-7-oxozeaenol**
449 The oxygen-induced retinopathy model was induced in rats as previously described (54). Briefly,
450 Sprague-Dawley litters (within 12 hours of birth; P0) and their nursing mothers were exposed to daily
451 cycles of 80% O_2 for 21 hours and room air for 3 hours in a custom-built and humidity-controlled (<
452 80%) chamber until P14. At P14 animals were returned to room air until P16 or P18, when they were
453 sacrificed to harvest retinae. An ProOx 110 oxygen controller (BioSpherix; Parish, NY) was used to
454 regulate and monitor the oxygen level. At P14, intravitreal injections were performed to administer
455 5Z-7-oxozeaenol visualizing with a microsurgical microscope. Under surface anesthesia, a puncture
456 in the superior temporal quadrant of the limbus was made by a 30-gauge needle. A hand-pulled glass
457 micropipette (Bio-Strategy, Australia) connected to a 10 µl Hamilton syringe (Hamilton Company,
458 Reno, NV) was inserted into the vitreous cavity, and one microliter of balanced salt solution containing
459 1% DMSO (as vehicle), low (18 ng) or high dose (90 ng) of 5Z-7-oxozeaenol was intravitreally
460 injected into the eye. For safety evaluation, Brown Norway rats were intravitreally injected with 1 µl
461 high dose (90 ng) of 5Z-7-oxozeaenol or vehicle. Eyes were excluded from the study if large backflow

462 after injection or severe hemorrhage were occurred. Electroretinography and optical coherence
463 tomography imaging evaluation was undertaken 28 days post-intravitreal injection in anesthetized
464 animals as previously described (55).
465
466 **Immunohistochemistry and vessel quantification**
467 Collection of donor samples was approved by the Human Research Ethics Committee of the Royal
468 Victorian Eye and Ear Hospital (HREC13/1151H) and carried out in accordance with the approved
469 guidelines. Post-mortem eye globes were obtained via the Lions Eye Donation Service (Royal
470 Victorian Eye and Ear Hospital, East Melbourne, VIC, Australia) and processed for paraffin
471 embedding and sectioning following standard histological procedures. Briefly, donated eyes were
472 isolated, fixed, and permeabilized. The cross sections were stained with anti-TAK1 (1:100; NBP1-
473 87819, Novus Biologicals, Littleton, CO) and anti-CD31 (1:25; M0823, DAKO, Jena, Germany)
474 primary antibody and then with the appropriate secondary antibodies. Images were digitized using a
475 confocal laser scanning microscope (FV3000; Olympus, Tokyo, Japan).
476 The rat retinal flat-mount were collected at P18 followed by retina dissection, staining overnight
477 with isolectin GS-IB_4 Alexa Fluor™ 488 conjugate (5 μg/mL; I21411, Life Technologies), anti-TAK1
478 (1:100; NBP1-87819, Novus Biologicals), or anti-Iba1 (1:300; 019-19741, FUJIFILM Wako
479 Chemicals, Richmond, VA), and then incubated with the appropriate secondary antibodies. The images
480 were captured by FV3000 confocal laser scanning microscope. The avascular (vaso-obliteration) and
481 neovascularized areas were quantified by two blinded assessors using Adobe Photoshop (San Jose,
482 CA) (56). Deep vessel area was analyzed by AngioTool software (National Institutes of Health,
483 Bethesda, MA) (57).
484
485 **Statistical analysis**
486 All data are expressed as mean ± SEM. Statistical analyses were performed with Graphpad Prism 7
487 (GraphPad, San Diego, CA) using student t-test for unpaired data, one-way or two-way ANOVA
488 wherever appropriate followed by Tukey's or Bonferroni's multiple comparisons test. P values < 0.05
489 were considered statistically significant.
490
491 **Data and resource availability statement**
492 The main datasets generated or analyzed during this study are included here in the article. Retinal RNA
493 profiles of OIR and control rats have been deposited in Gene Expression Omnibus and are accessible
494 through GEO Series accession number GSE104588
495 (https://www.ncbi.nlm.nih.gov/geo/query/acc.cgi?acc= GSE104588). The original Western Blot

images and the details of statistical analysis for this study are available in the supplementary information. Other original datasets will also be available to the research community upon reasonable request.

ACKNOWLEDGEMENTS

The authors thank UTAS CFF animal technicians, Karen Shiels, Keri Smith, Heather Howard, Lisa Harding and Danielle Eastley for their assistance with rat chamber operation. We also thank Dr Jacqueline Y.K. Leung for assistance with intravitreal injection, and Zheng He for assistance with retinal imaging. This work was supported by grants from the National Health and Medical Research Council of Australia (1061912, 1185600 and 1123329), the Ophthalmic Research Institute of Australia, the National Natural Science Foundation of China (82000902) and the Shenzhen Key Laboratory of Biomimetic Materials and Cellular Immunomodulation (ZDSYS20190902093409851). GJD was a Principal Research Fellow of NHMRC. The Centre for Eye Research Australia receives Operational Infrastructure Support from the Victorian Government.

COMPETING INTERESTS

The authors have declared that no competing interest exists.

AUTHOR CONTRIBUTIONS

Conceptualization- F-L.L., J-H.W., P.vW., G.J.D., G-S.L. Methodology- F-L.L., C.M., J-H.W., B.V.B., P.vW., G-S.L. Formal Analysis- F-L.L., J-H.W., J.C., R.C.B.W., B.V.B., G-S.L. Investigation- F-L.L., J-H.W., J.C., L.Z., Y-F.C., L.T., C.M., S.L., D.L., C-L.T., B.V.B. Resources- R.C.B.W., A.W.H., C-L.T., G.J.D., P-Y.W., G-S.L. Data Curation- F-L.L., J-H.W., J.C., G-S.L. Writing (Original Draft)- F-L.L., J-H.W., G-S.L. Writing (Review & Editing)- J.C., C.M., R.C.B.W., B.V.B., P.vW., G.J.D., P-Y.W. Project Administration- F-L.L., J-H.W., G-S.L. Funding Acquisition- L.T., G.J.D., P-Y.W., G-S.L. Project Supervision- G.S.L.

522 **REFERENCES**

523 1. Neely KA, and Gardner TW. Ocular neovascularization: clarifying complex interactions. *Am J*
524 *Pathol.* 1998;153(3):665-70.
525 2. Campochiaro PA. Retinal and choroidal neovascularization. *Journal of cellular physiology.*
526 2000;184(3):301-10.
527 3. Singer MA, Kermany DS, Waters J, Jansen ME, and Tyler L. Diabetic macular edema: it is
528 more than just VEGF. *F1000Res.* 2016;5.
529 4. Qazi Y, Maddula S, and Ambati BK. Mediators of ocular angiogenesis. *J Genet.*
530 2009;88(4):495-515.
531 5. Goldberg RB. Cytokine and cytokine-like inflammation markers, endothelial dysfunction, and
532 imbalanced coagulation in development of diabetes and its complications. *J Clin Endocrinol*
533 *Metab.* 2009;94(9):3171-82.
534 6. Demircan N, Safran BG, Soylu M, Ozcan AA, and Sizmaz S. Determination of vitreous
535 interleukin-1 (IL-1) and tumour necrosis factor (TNF) levels in proliferative diabetic
536 retinopathy. *Eye (Lond).* 2006;20(12):1366-9.
537 7. Capitao M, and Soares R. Angiogenesis and Inflammation Crosstalk in Diabetic Retinopathy.
538 *J Cell Biochem.* 2016;117(11):2443-53.
539 8. Murugeswari P, Shukla D, Rajendran A, Kim R, Namperumalsamy P, and Muthukkaruppan V.
540 Proinflammatory cytokines and angiogenic and anti-angiogenic factors in vitreous of patients
541 with proliferative diabetic retinopathy and eales' disease. *Retina.* 2008;28(6):817-24.
542 9. Stevenson W, Cheng SF, Dastjerdi MH, Ferrari G, and Dana R. Corneal neovascularization and
543 the utility of topical VEGF inhibition: ranibizumab (Lucentis) vs bevacizumab (Avastin). *Ocul*
544 *Surf.* 2012;10(2):67-83.
545 10. Aveleira CA, Lin CM, Abcouwer SF, Ambrosio AF, and Antonetti DA. TNF-alpha signals
546 through PKCzeta/NF-kappaB to alter the tight junction complex and increase retinal
547 endothelial cell permeability. *Diabetes.* 2010;59(11):2872-82.
548 11. Clauss M, Sunderkotter C, Sveinbjornsson B, Hippenstiel S, Willuweit A, Marino M, et al. A
549 permissive role for tumor necrosis factor in vascular endothelial growth factor-induced
550 vascular permeability. *Blood.* 2001;97(5):1321-9.
551 12. Yoshida S, Yoshida A, and Ishibashi T. Induction of IL-8, MCP-1, and bFGF by TNF-alpha in
552 retinal glial cells: implications for retinal neovascularization during post-ischemic
553 inflammation. *Graefes Arch Clin Exp Ophthalmol.* 2004;242(5):409-13.
554 13. Joussen AM, Poulaki V, Mitsiades N, Kirchhof B, Koizumi K, Dohmen S, et al. Nonsteroidal
555 anti-inflammatory drugs prevent early diabetic retinopathy via TNF-alpha suppression. *FASEB*
556 *journal : official publication of the Federation of American Societies for Experimental Biology.*
557 2002;16(3):438-40.
558 14. Sato S, Sanjo H, Takeda K, Ninomiya-Tsuji J, Yamamoto M, Kawai T, et al. Essential function
559 for the kinase TAK1 in innate and adaptive immune responses. *Nat Immunol.* 2005;6(11):1087-

560 95.
561 15. Shim JH, Xiao C, Paschal AE, Bailey ST, Rao P, Hayden MS, et al. TAK1, but not TAB1 or
562 TAB2, plays an essential role in multiple signaling pathways in vivo. *Genes Dev.*
563 2005;19(22):2668-81.
564 16. Mihaly SR, Ninomiya-Tsuji J, and Morioka S. TAK1 control of cell death. *Cell death and*
565 *differentiation.* 2014;21(11):1667-76.
566 17. Scarneo SA, Mansourati A, Eibschutz LS, Totzke J, Roques JR, Loiselle D, et al. Genetic and
567 pharmacological validation of TAK1 inhibition in macrophages as a therapeutic strategy to
568 effectively inhibit TNF secretion. *Sci Rep.* 2018;8(1):17058.
569 18. Harikumar KB, Sung B, Tharakan ST, Pandey MK, Joy B, Guha S, et al. Sesamin manifests
570 chemopreventive effects through the suppression of NF-kappa B-regulated cell survival,
571 proliferation, invasion, and angiogenic gene products. *Mol Cancer Res.* 2010;8(5):751-61.
572 19. Naito H, Iba T, Wakabayashi T, Tai-Nagara I, Suehiro JI, Jia W, et al. TAK1 Prevents
573 Endothelial Apoptosis and Maintains Vascular Integrity. *Dev Cell.* 2019;48(2):151-66 e7.
574 20. Morioka S, Inagaki M, Komatsu Y, Mishina Y, Matsumoto K, and Ninomiya-Tsuji J. TAK1
575 kinase signaling regulates embryonic angiogenesis by modulating endothelial cell survival and
576 migration. *Blood.* 2012;120(18):3846-57.
577 21. Schoneberg J, De Lorenzi F, Theek B, Blaeser A, Rommel D, Kuehne AJC, et al. Engineering
578 biofunctional in vitro vessel models using a multilayer bioprinting technique. *Sci Rep.*
579 2018;8(1):10430.
580 22. Subramanian A, Tamayo P, Mootha VK, Mukherjee S, Ebert BL, Gillette MA, et al. Gene set
581 enrichment analysis: a knowledge-based approach for interpreting genome-wide expression
582 profiles. *Proc Natl Acad Sci U S A.* 2005;102(43):15545-50.
583 23. Ninomiya-Tsuji J, Kajino T, Ono K, Ohtomo T, Matsumoto M, Shiina M, et al. A resorcylic
584 acid lactone, 5Z-7-oxozeaenol, prevents inflammation by inhibiting the catalytic activity of
585 TAK1 MAPK kinase kinase. *J Biol Chem.* 2003;278(20):18485-90.
586 24. Hackett SF, Wiegand S, Yancopoulos G, and Campochiaro PA. Angiopoietin-2 plays an
587 important role in retinal angiogenesis. *J Cell Physiol.* 2002;192(2):182-7.
588 25. Fechtner S, Fox DA, and Ahmed S. Transforming growth factor beta activated kinase 1: a
589 potential therapeutic target for rheumatic diseases. *Rheumatology (Oxford).* 2017;56(7):1060-
590 8.
591 26. Mukhopadhyay H, and Lee NY. Multifaceted roles of TAK1 signaling in cancer. *Oncogene.*
592 2020;39(7):1402-13.
593 27. Yang Y, Wu, J, and Wang, J.K. A database and functional annotation of NF-κB target genes. *Int*
594 *J Clin Exp Med.* 2016;9(5):7986-95.
595 28. Ghosh S, and Karin M. Missing pieces in the NF-kappaB puzzle. *Cell.* 2002;109 Suppl:S81-
596 96.
597 29. Li J, Liang C, Zhang ZK, Pan X, Peng S, Lee WS, et al. TAK1 inhibition attenuates both

598 inflammation and fibrosis in experimental pneumoconiosis. *Cell Discov.* 2017;3:17023.
599 30. Yang L, Joseph S, Sun T, Hoffmann J, Thevissen S, Offermanns S, et al. TAK1 regulates
600 endothelial cell necroptosis and tumor metastasis. *Cell death and differentiation.*
601 2019;26(10):1987-97.
602 31. Dai L, Aye Thu C, Liu XY, Xi J, and Cheung PC. TAK1, more than just innate immunity.
603 *IUBMB Life.* 2012;64(10):825-34.
604 32. Onodera Y, Teramura T, Takehara T, Shigi K, and Fukuda K. Reactive oxygen species induce
605 Cox-2 expression via TAK1 activation in synovial fibroblast cells. *FEBS Open Bio.*
606 2015;5:492-501.
607 33. Xie M, Zhang D, Dyck JR, Li Y, Zhang H, Morishima M, et al. A pivotal role for endogenous
608 TGF-beta-activated kinase-1 in the LKB1/AMP-activated protein kinase energy-sensor
609 pathway. *Proc Natl Acad Sci U S A.* 2006;103(46):17378-83.
610 34. Sakurai H. Targeting of TAK1 in inflammatory disorders and cancer. *Trends in*
611 *pharmacological sciences.* 2012;33(10):522-30.
612 35. Sabio G, and Davis RJ. TNF and MAP kinase signalling pathways. *Semin Immunol.*
613 2014;26(3):237-45.
614 36. Landry J, and Huot J. Regulation of actin dynamics by stress-activated protein kinase 2
615 (SAPK2)-dependent phosphorylation of heat-shock protein of 27 kDa (Hsp27). *Biochem Soc*
616 *Symp.* 1999;64:79-89.
617 37. Munoz-Chapuli R, Quesada AR, and Angel Medina M. Angiogenesis and signal transduction
618 in endothelial cells. *Cell Mol Life Sci.* 2004;61(17):2224-43.
619 38. Tang M, Wei X, Guo Y, Breslin P, Zhang S, Zhang S, et al. TAK1 is required for the survival
620 of hematopoietic cells and hepatocytes in mice. *The Journal of experimental medicine.*
621 2008;205(7):1611-9.
622 39. Wu J, Powell F, Larsen NA, Lai Z, Byth KF, Read J, et al. Mechanism and in vitro
623 pharmacology of TAK1 inhibition by (5Z)-7-Oxozeaenol. *ACS chemical biology.*
624 2013;8(3):643-50.
625 40. Zhang D, Yan H, Li H, Hao S, Zhuang Z, Liu M, et al. TGFbeta-activated Kinase 1 (TAK1)
626 Inhibition by 5Z-7-Oxozeaenol Attenuates Early Brain Injury after Experimental Subarachnoid
627 Hemorrhage. *The Journal of biological chemistry.* 2015;290(32):19900-9.
628 41. Lu L, Zhang X, Tong H, Zhang W, Xu P, and Qu S. Central Administration of 5Z-7-Oxozeaenol
629 Protects Experimental Autoimmune Encephalomyelitis Mice by Inhibiting Microglia
630 Activation. *Front Pharmacol.* 2017;8:789.
631 42. Merson TD, Binder MD, and Kilpatrick TJ. Role of cytokines as mediators and regulators of
632 microglial activity in inflammatory demyelination of the CNS. *Neuromolecular Med.*
633 2010;12(2):99-132.
634 43. White BJ, Tarabishy S, Venna VR, Manwani B, Benashski S, McCullough LD, et al. Protection
635 from cerebral ischemia by inhibition of TGFbeta-activated kinase. *Exp Neurol.*

636 2012;237(1):238-45.
637 44. Ivshina M, Alexandrov IM, Vertii A, Doxsey S, and Richter JD. CPEB regulation of TAK1
638 synthesis mediates cytokine production and the inflammatory immune response. *Mol Cell Biol.*
639 2015;35(3):610-8.
640 45. Ireland DJ, Kemp MW, Miura Y, Saito M, Newnham JP, and Keelan JA. Intra-amniotic
641 pharmacological blockade of inflammatory signalling pathways in an ovine chorioamnionitis
642 model. *Mol Hum Reprod.* 2015;21(5):479-89.
643 46. Neubert M, Ridder DA, Bargiotas P, Akira S, and Schwaninger M. Acute inhibition of TAK1
644 protects against neuronal death in cerebral ischemia. *Cell death and differentiation.*
645 2011;18(9):1521-30.
646 47. Bettermann K, Vucur M, Haybaeck J, Koppe C, Janssen J, Heymann F, et al. TAK1 suppresses
647 a NEMO-dependent but NF-kappaB-independent pathway to liver cancer. *Cancer Cell.*
648 2010;17(5):481-96.
649 48. Omori E, Morioka S, Matsumoto K, and Ninomiya-Tsuji J. TAK1 regulates reactive oxygen
650 species and cell death in keratinocytes, which is essential for skin integrity. *J Biol Chem.*
651 2008;283(38):26161-8.
652 49. Bui BV, and Fortune B. Ganglion cell contributions to the rat full-field electroretinogram. *J*
653 *Physiol.* 2004;555(Pt 1):153-73.
654 50. Cao H, Lu J, Du J, Xia F, Wei S, Liu X, et al. TAK1 inhibition prevents the development of
655 autoimmune diabetes in NOD mice. *Sci Rep.* 2015;5:14593.
656 51. Tan L, Gurbani D, Weisberg EL, Jones DS, Rao S, Singer WD, et al. Studies of TAK1-centered
657 polypharmacology with novel covalent TAK1 inhibitors. *Bioorg Med Chem.* 2017;25(4):1320-
658 8.
659 52. Butler A, Hoffman P, Smibert P, Papalexi E, and Satija R. Integrating single-cell transcriptomic
660 data across different conditions, technologies, and species. *Nat Biotechnol.* 2018;36(5):411-20.
661 53. Stuart T, Butler A, Hoffman P, Hafemeister C, Papalexi E, Mauck WM, 3rd, et al.
662 Comprehensive Integration of Single-Cell Data. *Cell.* 2019;177(7):1888-902 e21.
663 54. Penn JS, Tolman BL, and Henry MM. Oxygen-induced retinopathy in the rat: relationship of
664 retinal nonperfusion to subsequent neovascularization. *Invest Ophthalmol Vis Sci.*
665 1994;35(9):3429-35.
666 55. Bee YS, Tu L, Sheu SJ, Lin HC, Tang JH, Wang JH, et al. Gene Delivery of Calreticulin Anti-
667 Angiogenic Domain Attenuates the Development of Choroidal Neovascularization in Rats.
668 *Hum Gene Ther.* 2017;28(5):403-14.
669 56. Connor KM, Krah NM, Dennison RJ, Aderman CM, Chen J, Guerin KI, et al. Quantification
670 of oxygen-induced retinopathy in the mouse: a model of vessel loss, vessel regrowth and
671 pathological angiogenesis. *Nat Protoc.* 2009;4(11):1565-73.
672 57. Zudaire E, Gambardella L, Kurcz C, and Vermeren S. A computational tool for quantitative
673 analysis of vascular networks. *PLoS One.* 2011;6(11):e27385.

674 58. Zhao D, Nguyen CT, Wong VH, Lim JK, He Z, Jobling AI, et al. Characterization of the
675 Circumlimbal Suture Model of Chronic IOP Elevation in Mice and Assessment of Changes in
676 Gene Expression of Stretch Sensitive Channels. *Front Neurosci.* 2017;11:41.
677

678

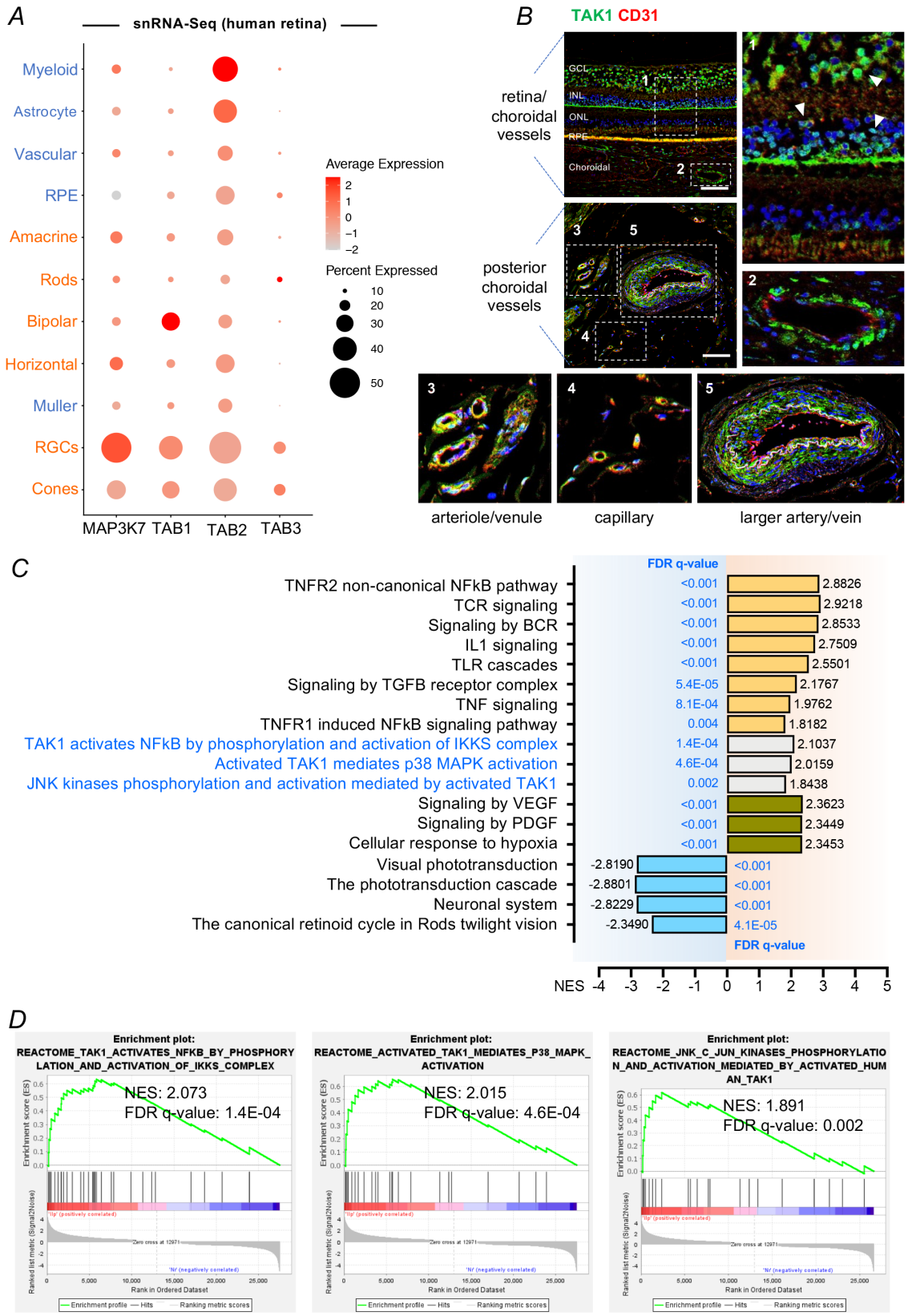

Fig. 1 Characterization of TAK1 expression in patients with retinal neovascularization associated with proliferative diabetic retinopathy.

682 (A) Single nuclei RNAseq (snRNAseq) characterization of TAK1 (MAP3K7) expression in normal
683 human retina. TAK1 and TAK1-associated proteins (TAB1-3) were expressed in most neural (red)
684 and non-neural (blue) cells in the retina, including cell associated with the retinal vasculature. (B)
685 Characterization of TAK1 expression in the normal human retina. Endothelial cells were labelled with
686 CD31 (red) and counterstained with TAK1 (green) in retinal section. Apart from neural cells, TAK1
687 expression was also found in vascular endothelial cells, especially in retinal capillaries (3 and 4). Scale
688 bar: 100 µm. (C) Gene-set enrichment analysis (GSEA) indicated that TAK1 upstream pathways
689 including IL1, TNF, TCR, BCR, TLR, TNFR, or TGFβ signaling (Reactome Pathway Database) were
690 positively enriched in retinal samples from patients with retinal neovascularization due to proliferative
691 diabetic retinopathy. Engagement of TAK1-activated NFκB, p38 MAPK and JNK pathways as well
692 as negative impact on retinal neural functions were also identified. (D) GSEA Enrichment plots
693 illustration of gene set involved in TAK1-NFκB, TAK1-p38 MAPK and TAK1-JNK pathways in the
694 retina of patients with proliferative diabetic retinopathy. GCL: ganglion cell layer; INL: inner nuclear
695 layer; ONL: outer nuclear layer; RPE: retinal pigment epithelium; NSE: normalized enrichment score;
696 FDR: false discovery rate.
697
698

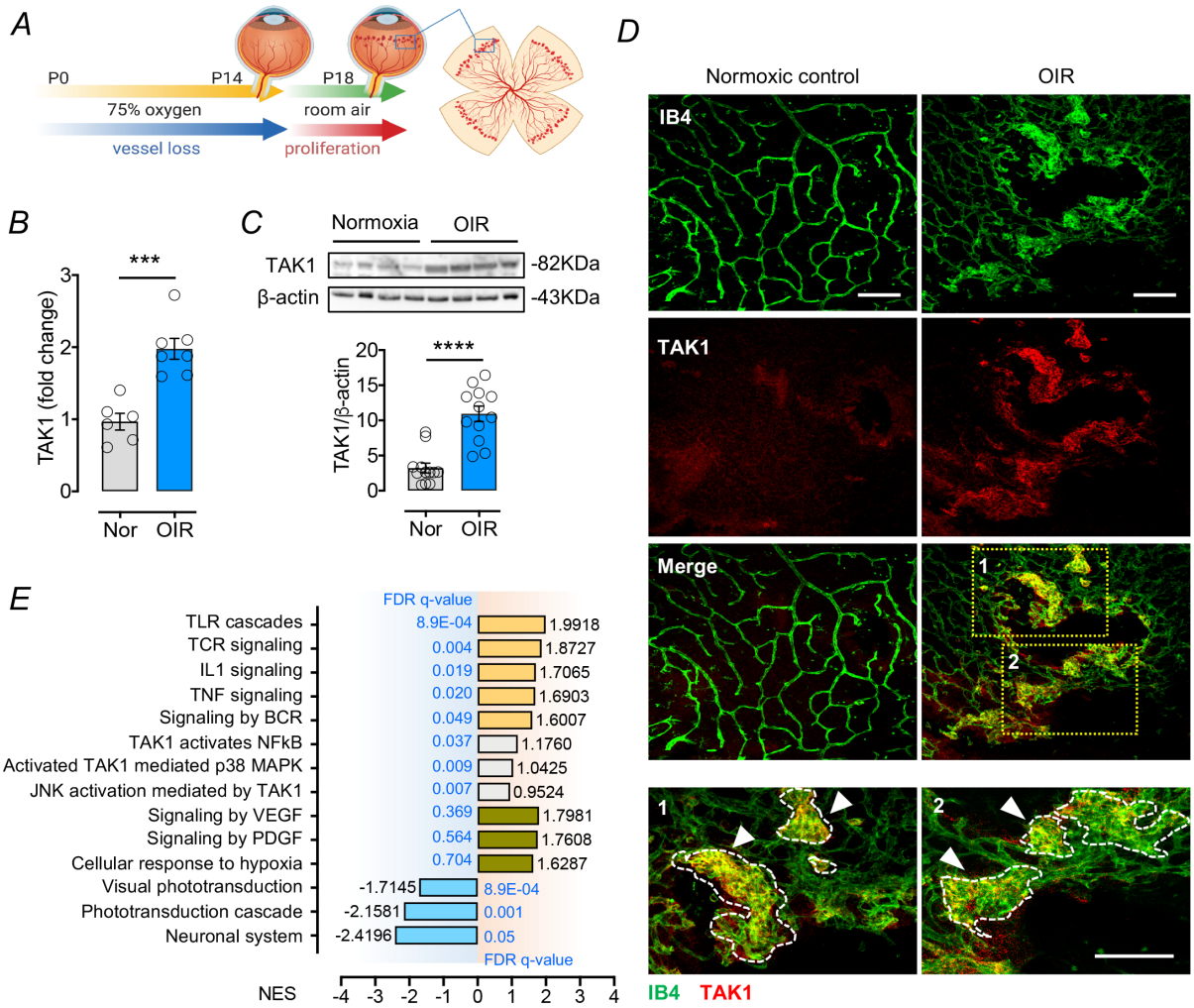

Fig. 2 Involvement of TAK1 in pathological retinal angiogenesis in a rat model of oxygen-induced retinopathy. (A) Schematic diagram of the Sprague-Dawley rat model of oxygen-induced retinopathy (OIR). Neonatal rats were exposed to 80% of oxygen for 21 hours each day from postnatal day 0 (P0) to P14. Rats were returned to room air from P14 to P18. Vessel loss was induced during oxygen exposure and retinal angiogenesis could be induced after rats returned to room air. (B) qPCR analysis of *TAK1* expression in OIR at P18 as compared with the normoxic control (Nor) group (n = 6-7). (C) Western blot analysis of TAK1 expression in OIR at P18 compared with normoxic control group (n = 10-12). Representative immunoblotting from 4 independent samples were shown for normoxic control (lanes 1-4) and OIR group (lanes 5-8). (D) Immunobiological staining indicated expression of TAK1 in the pathological vessel. Vasculature were visualized by isolectin GS-IB4 labelling (green) and counterstained with TAK1 (red) in retinal whole mount. Arrowheads indicate vessel tufts. Scale bar: 100 μm. (E) GSEA indicated that most of TAK1 upstream pathways including TNF, IL1, TCR, BCR, TLR, and VEGF pathways (from Reactome Pathway Database) were positively enriched in OIR at P18. Engagement of TAK1-activated NFκB, p38 MAPK and JNK pathways as well as negative impact on retinal neural functions were also identified. Group data are shown as means ± SEM. Statistical analysis was undertaken with two-tailed unpaired t-test; ***$P < 0.001$, ****$P < 0.0001$. NSE: normalized enrichment score; FDR: false discovery rate.

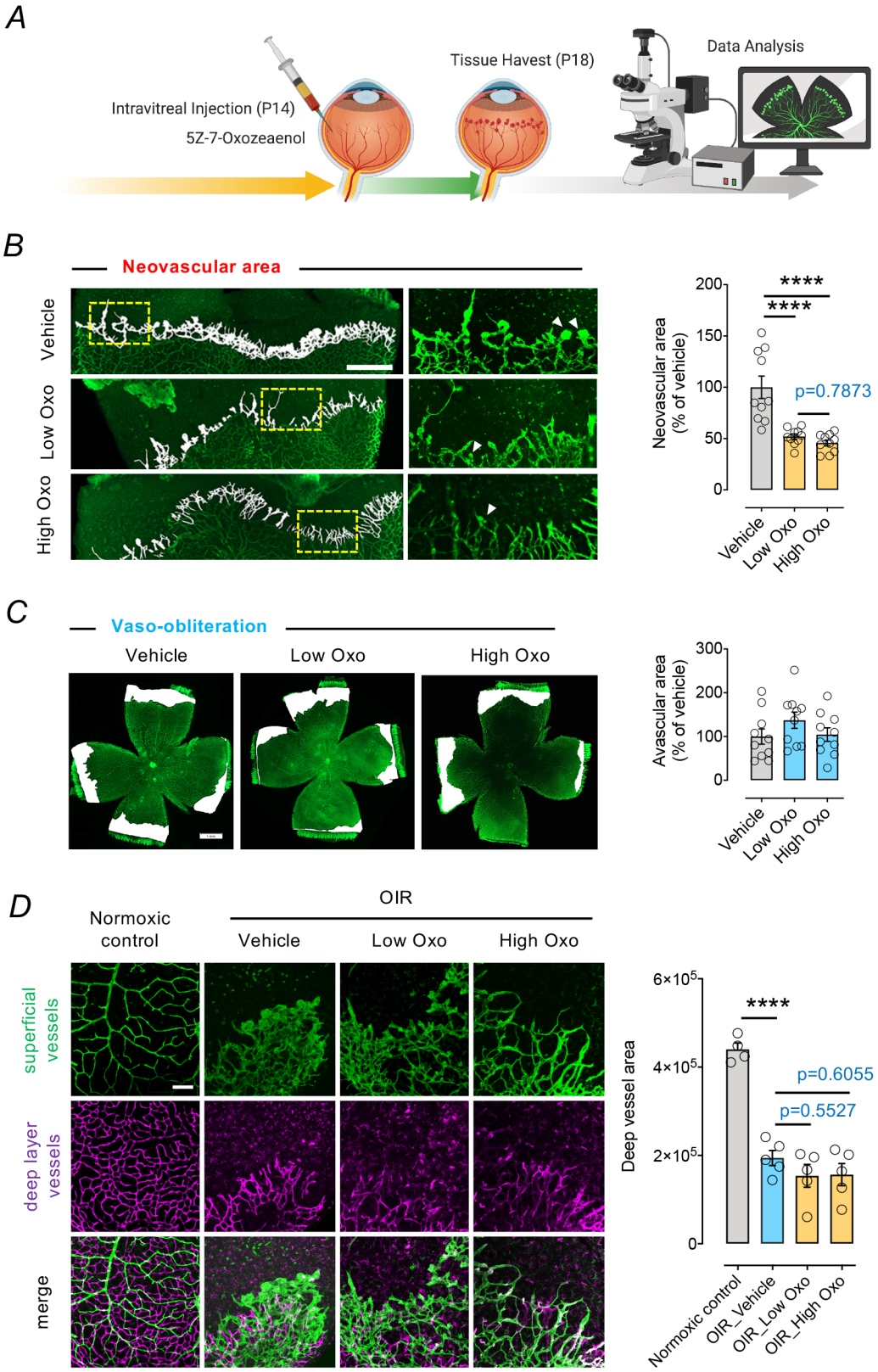

Fig. 3 TAK1 Inhibition by 5Z-7-oxozeaenol suppressed retinal angiogenesis in OIR rats. (A) Experimental protocol for 5Z-7-oxozeaenol treatment in the OIR rat model. A single intravitreal injection of vehicle, low (18 ng) or high (90 ng) dose of 5Z-7-oxozeaenol was given to Sprague-

721 Dawley OIR rats at P14, followed by quantitative analysis of retinal neovascularization of flat mounted
722 retinae at P18. (B) Retinal neovascularization is highlighted in white, and insets show selected areas
723 at high magnification. Arrowheads indicate vessel tufts. Retinal neovascularization was quantified
724 from 10 individual retinas per group. Scale bar: 500 µm. (C) Vaso-obliteration was simultaneously
725 evaluated with the same samples analyzed in Fig. 3B. The white areas represent the avascular area in
726 the retina. No significant difference was observed between groups (n = 10). Scale bar: 1 mm. (D)
727 Vessel area of superficial and deep vascular layers was quantified in P18 control (n = 4) and OIR rats
728 following a single intravitreal injection of vehicle, low or high dose of 5Z-7-oxozeaenol at P14 (n = 5
729 each group). Scale bar: 100 µm. Group data are shown as means ± SEM. Statistical analysis was
730 undertaken with one-way ANOVA and Tukey's multiple comparison test; ****$P < 0.0001$.
731

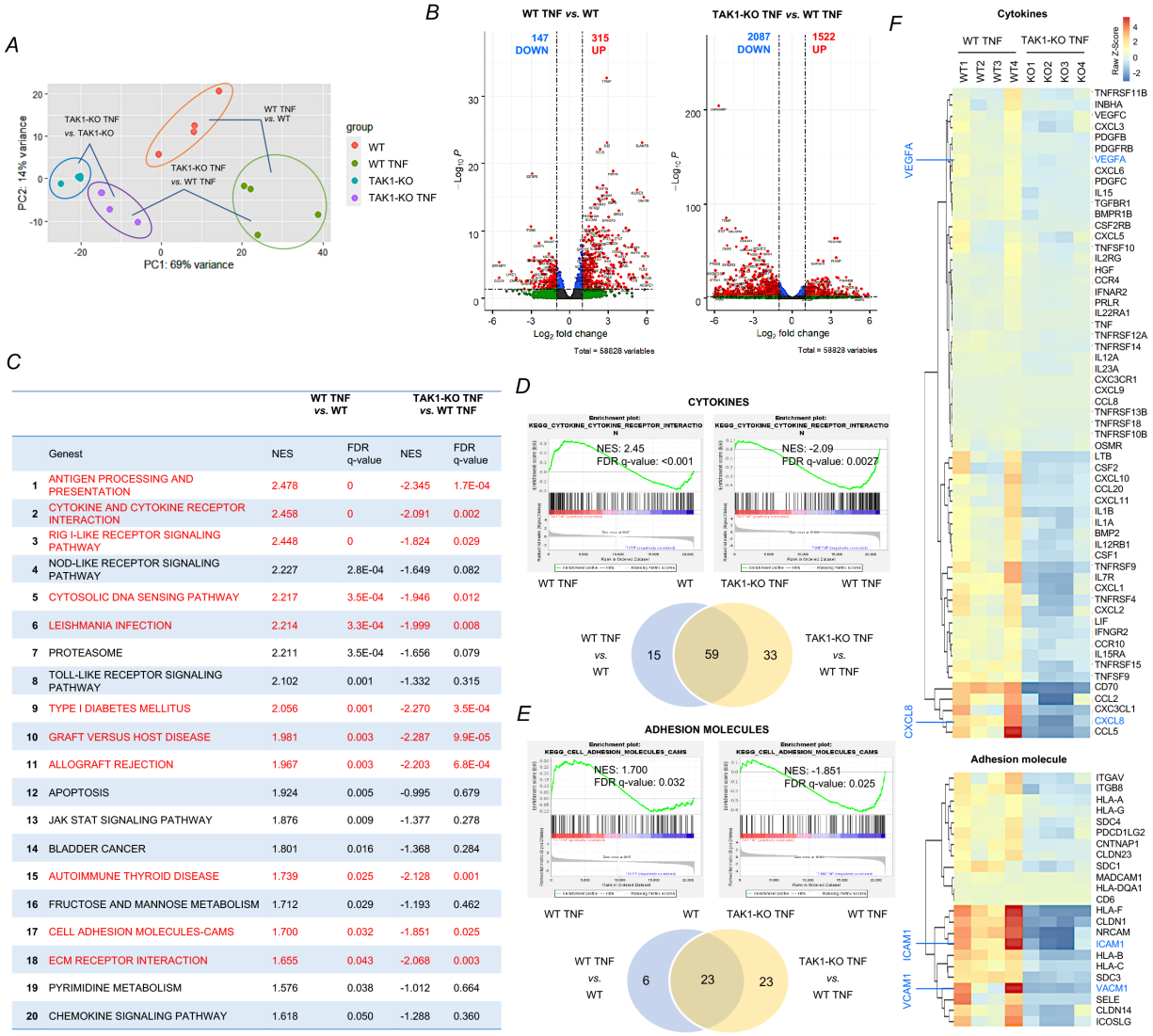

	Genest	WT TNF vs. WT NES	WT TNF vs. WT FDR q-value	TAK1-KO TNF vs. WT TNF NES	TAK1-KO TNF vs. WT TNF FDR q-value
1	ANTIGEN PROCESSING AND PRESENTATION	2.478	0	-2.345	1.7E-04
2	CYTOKINE AND CYTOKINE RECEPTOR INTERACTION	2.458	0	-2.091	0.002
3	RIG I-LIKE RECEPTOR SIGNALING PATHWAY	2.448	0	-1.824	0.029
4	NOD-LIKE RECEPTOR SIGNALING PATHWAY	2.227	2.8E-04	-1.649	0.082
5	CYTOSOLIC DNA SENSING PATHWAY	2.217	3.5E-04	-1.946	0.012
6	LEISHMANIA INFECTION	2.214	3.3E-04	-1.999	0.008
7	PROTEASOME	2.211	3.5E-04	-1.656	0.079
8	TOLL-LIKE RECEPTOR SIGNALING PATHWAY	2.102	0.001	-1.332	0.315
9	TYPE I DIABETES MELLITUS	2.056	0.001	-2.270	3.5E-04
10	GRAFT VERSUS HOST DISEASE	1.981	0.003	-2.287	9.9E-05
11	ALLOGRAFT REJECTION	1.967	0.003	-2.203	6.8E-04
12	APOPTOSIS	1.924	0.005	-0.995	0.679
13	JAK STAT SIGNALING PATHWAY	1.876	0.009	-1.377	0.278
14	BLADDER CANCER	1.801	0.016	-1.368	0.284
15	AUTOIMMUNE THYROID DISEASE	1.739	0.025	-2.128	0.001
16	FRUCTOSE AND MANNOSE METABOLISM	1.712	0.029	-1.193	0.462
17	CELL ADHESION MOLECULES-CAMS	1.700	0.032	-1.851	0.025
18	ECM RECEPTOR INTERACTION	1.655	0.043	-2.068	0.003
19	PYRIMIDINE METABOLISM	1.576	0.038	-1.012	0.664
20	CHEMOKINE SIGNALING PATHWAY	1.618	0.050	-1.288	0.360

Fig. 4 TAK1 deletion inhibits the expression of cytokines and cell adhesion molecules induced by TNFα in human microvascular endothelial cells.
(A) Principal components analysis of RNA-seq data of wild-type (WT) endothelial cells (TIMEs), WT TIMEs treated with TNFα, TAK1 knockout (TAK1-KO) TIMEs, and TAK1-KO TIMEs treated with TNFα. Each dot represents an experimental replicate. (A) Volcano plots show genes that were significantly changed in both WT and TAK1-KO TIMEs when stimulated by TNFα. Red dots refer to genes showing a log2|fold change| > 1 and FDR < 0.05. Labels indicate significantly up-regulated genes in each data set. (C) GSEA of the top 20 KEGG gene sets in the two groups. Significantly enriched gene sets in WT TNF set (WT TNF vs. WT) (positive NES) and less enriched ones in TAK1-KO set (TAK1-KO TNF vs. WT TNF) (negative NES) are highlighted in red. False discovery rate (FDR) q-value < 0.05 was considered to be statistically significant. (D) GSEA plots for gene sets with Gene Ontology (GO) term "CYTOKINE AND CYTOKINE RECEPTOR INTERACTION" (related to cytokines) in the two groups. The Venn diagram shows the number of genes from the cytokine gene sets in the respective and overlapping areas of the two groups. (E) GSEA plots for gene sets with GO term "CELL ADHESION MOLECULES-CAMS" (related to adhesion molecules) in the two groups. The Venn diagram shows the number of genes from the chemokine gene sets in respective and overlapping areas of the two groups. (F) Heat map generated from the identified overlapping areas of "cytokines (n = 59)" "adhesion molecules (n = 23)" gene sets based on RNA-Seq read counts.

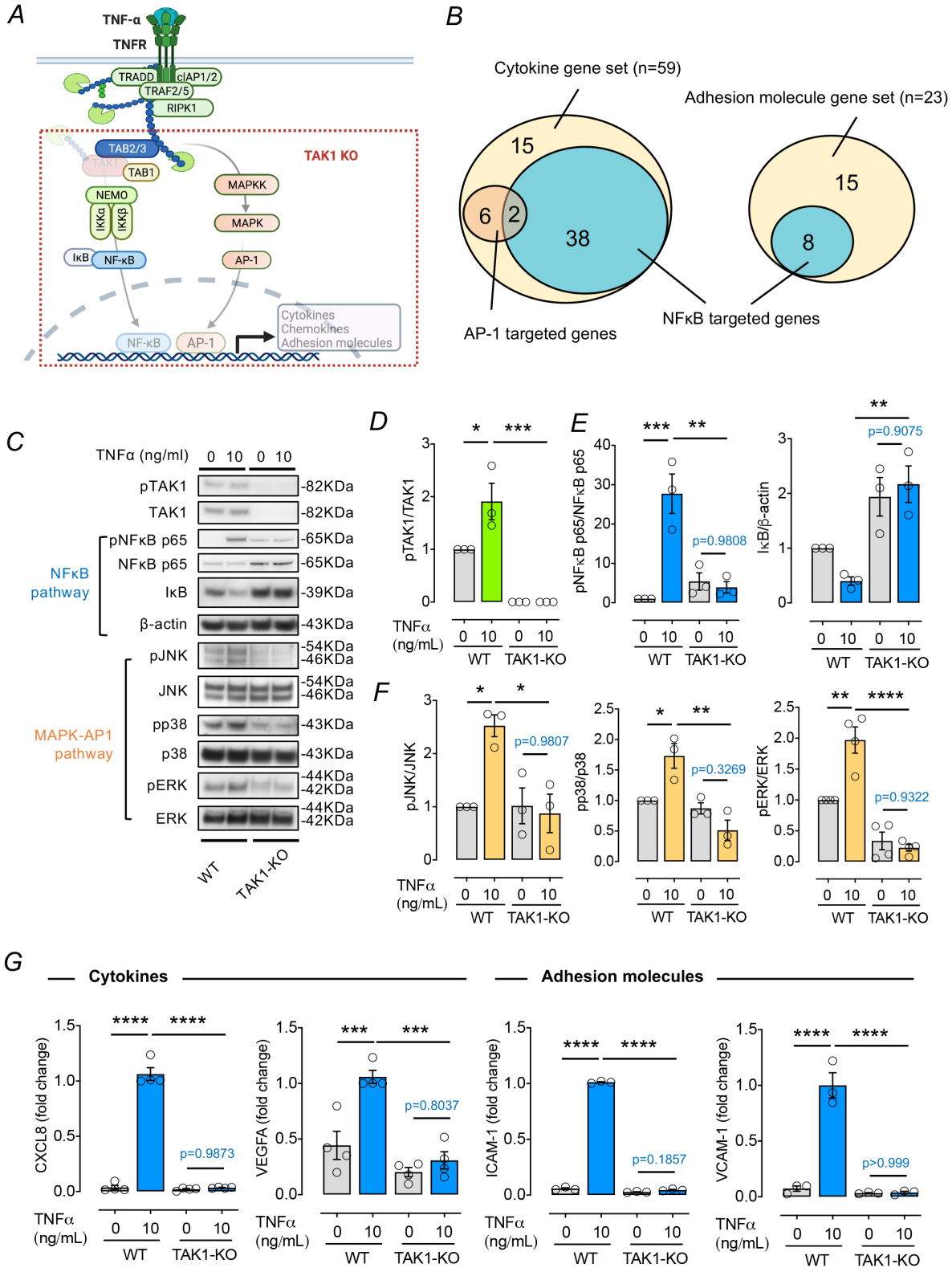

Fig. 5 TAK1 deletion prevents TNFα-induced inflammatory cascade through the NFκB and MAPK pathway in human microvascular endothelial cells.

(A) Schematic diagram of TNFα-TAK1 signaling. Upon TNFα stimulation, TAK1 binds to the polyubiquitin chain though TAB2, and activates the IKK complex, leading to the activation of NF-κB.

TAK1 also activates MAPKs cascades. NFκB and MAPKs/AP-1 induce expression of inflammatory cytokines and cell adhesion proteins. (B) The Venn diagram respectively shows the number of genes from the "cytokine" and "adhesion molecule" gene sets, and the overlap indicates the number of genes directly targeted by NFκB or AP-1. (C) Western blot characterization of the TNFα-induced phosphorylation of TAK1, NFκB, and MAPKs proteins in TAK1 knockout (TAK1-KO) TIMEs. Wild-type (WT) and TAK1-KO TIMEs were stimulated by TNFα (10 ng/ml) for 10 minutes. Activation of TAK1, NFκB p65, IκB, JNK, p38, and ERK assessed using western blot (n = 3-4). Genetic TAK1 deletion reduced TAK1 expression (D) and impaired NFκB (NFκB p65 and IκB) (E) and MAPK (p38, JNK, and ERK) (F) signaling in TIMEs treated with TNFα. (G) qPCR results revealed that TAK1 deletion suppressed the expression of selected cytokines (*CXCL8* and *VEGFA)* and cell adhesion molecules (*ICAM-1* and *VCAM-1)* in TIMEs stimulated with TNFα for 24 hours (n = 3-4). Group data are shown as means ± SEM. Statistical analysis was undertaken with one-way ANOVA and Tukey's multiple comparison test; $^{*}P < 0.05$, $^{**}P < 0.01$, $^{***}P < 0.001$, $^{****}P < 0.0001$.

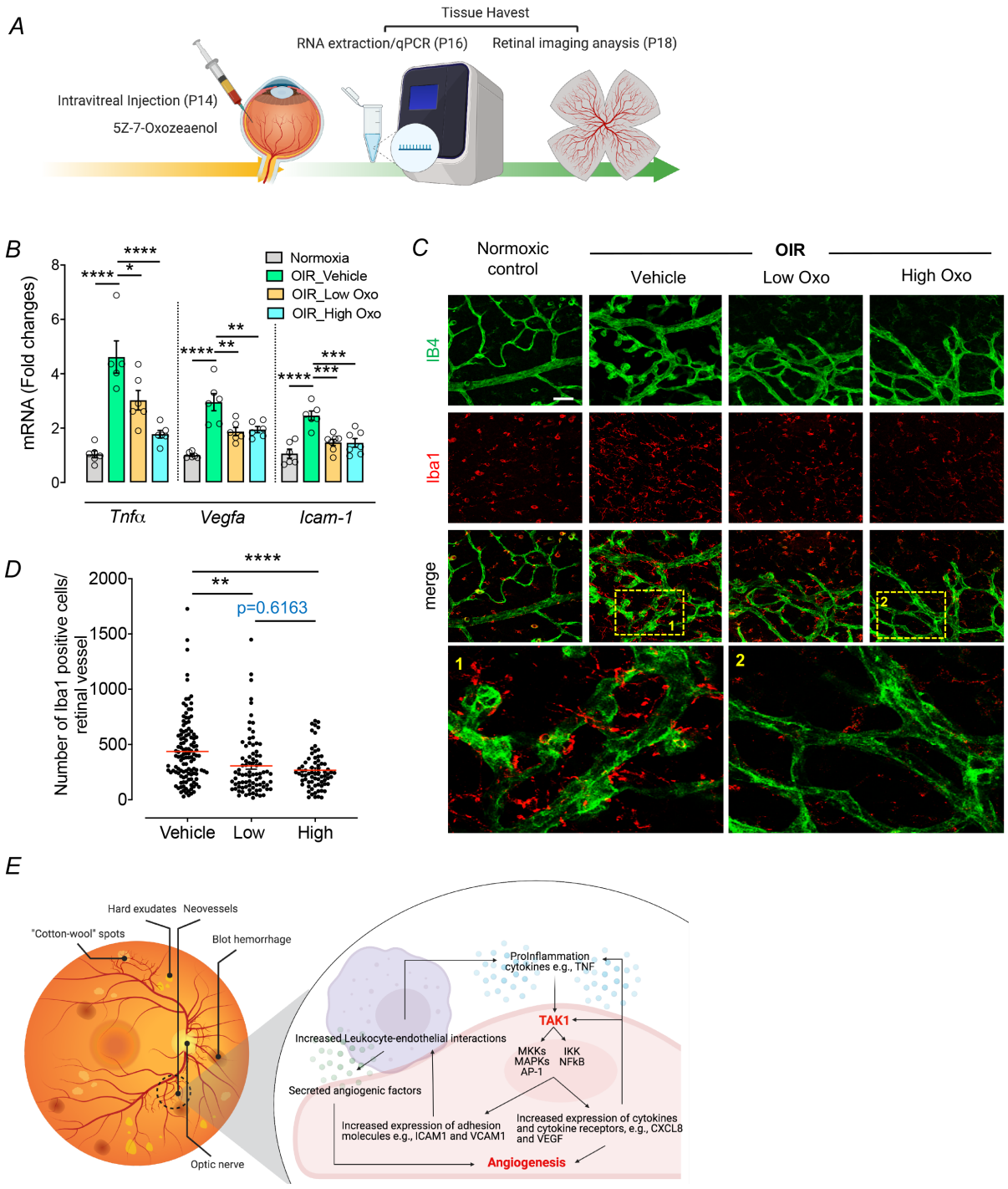

Fig. 6 TAK1 inhibition by 5Z-7-oxozeaenol decreased inflammatory gene expression and adhesion of microglia to vessels in OIR.

(A) Experimental protocol for 5Z-7-oxozeaenol treatment in the OIR rat model. A single intravitreal injection of vehicle, low (18 ng) or high (90 ng) dose of 5Z-7-oxozeaenol was given to Sprague-Dawley OIR rats at P14, and retinae were collected for qPCR and immunostaining at P16 and P18. (B) Intravitreal injection of 5Z-7-oxozeaenol in OIR rats at P14 inhibited *TNFα*, *VEGFA* and *ICAM-1* gene expression assessed using qPCR (n = 5-7). (C) Representative images of microglial adhesion to the vascular surface in a retina from a control rat and OIR rats that had a single intravitreal injection of vehicle, low or high dose of 5Z-7-oxozeaenol (Oxo). Vessels were visualized with isolectin GS-IB4

780 staining (green), and distribution of microglia was immunolabeled with Iba-1 (red). Scale bar: 50 μm.
781 (D) Quantitative analysis of microglial number relative to retinal vessel area in vehicle or 5Z-7-
782 oxozeaenol treated OIR rats (n = 7-10; 10 images from each retina were shown as separated dot plot).
783 (E) Schematic diagram for the role of TAK1 signaling in microvascular endothelial cells.
784 Proinflammatory cytokines such as TNFα can activate TAK1 in microvascular endothelial cells, and
785 TAK1/TAB1/TAB2-3 complex can lead to activation of NFκB and MAPKs/AP-1 cascades. NFκB and
786 MAPKs/AP-1 induce expression of "cytokines" and "adhesion proteins", thereby triggering the
787 "inflammatory cycle" and "leukostasis", and leading to retinal neovascularization. Group data are
788 shown as means ± SEM. Statistical analysis was undertaken with one-way ANOVA and Tukey's
789 multiple comparison test; *$P < 0.05$, **$P < 0.01$, ***$P < 0.001$, ****$P < 0.0001$.
790

791 **SUPPLEMENTARY MATERIALS**

792 **Table S1** Effects on the expression of enriched genes mediated by NFκB or AP-1 signaling in "TAK1-
793 KO TNF *vs.* WT TNF" data set compared to "WT TNF *vs.* WT" data set.
794

Gene name	WT TNF vs WT		TAK1-KO TNF vs TAK1-KO TNF		NFkB or AP-1 targeted gene
	log2FoldChange	FDR q-value	log2FoldChange	FDR q-value	
Cytokines-Cytokine Receptors (n=58)					
IL1B	4.35670	3.94E-11	-4.41950	2.40E-05	NFκB
CXCL1	1.83710	7.24E-11	-2.34930	3.41E-04	NFκB
IL1A	3.29810	5.17E-10	-1.87860	6.40E-03	NFκB
VEGFC	1.72730	1.06E-09	-0.81200	1.29E-02	NFκB
TNFRSF9	6.36650	1.62E-09	-5.03510	2.97E-05	None
TNFRSF4	4.86660	1.03E-08	-2.56130	9.43E-03	None
CCL2	4.79430	2.35E-08	-3.10600	2.47E-02	NFκB
CCL5	6.50100	1.47E-07	-6.05740	5.44E-07	NFκB
CXCL2	2.68970	8.93E-07	-2.39200	1.56E-02	NFκB
CD70	1.74470	1.94E-06	-8.39220	4.56E-13	NFκB
PDGFB	1.05430	2.71E-06	-0.63160	4.20E-04	NFκB
LIF	2.06620	8.24E-06	-2.46700	2.83E-10	NFκB
CXCL5	4.02040	9.25E-06	-1.43094	3.26E-01	None
CXCL6	3.20050	1.13E-05	-3.24340	1.99E-05	NFκB
CXCL8	3.40100	2.62E-05	-4.62360	1.53E-07	NFκB
CXCL3	2.83370	3.02E-05	-1.95808	2.94E-01	NA
CCR10	1.38350	5.53E-05	-1.94630	6.67E-09	AP-1
CXCL10	9.88480	6.15E-05	-5.92910	5.15E-03	NFκB
CSF1	1.54050	9.12E-05	-1.47410	2.91E-09	NFκB
CXCL11	8.86230	1.07E-04	-5.92440	9.63E-03	NFκB
IL12RB1	2.38450	1.60E-04	-2.56180	6.75E-08	NFκB
IFNGR2	1.06720	2.21E-04	-1.20550	3.02E-09	NFκB
VEGFA	0.97810	2.91E-04	-0.96540	5.89E-07	NFκB
CX3CL1	4.93410	3.00E-04	-5.75310	1.09E-05	NFκB
CCL20	5.98070	3.08E-04	-6.66700	2.81E-04	NFκB
TNFRSF11B	2.27490	5.60E-04	-1.22159	2.09E-01	None
LTB	5.02310	8.03E-04	-5.28530	4.51E-07	NFκB
IL15RA	0.95000	1.28E-03	-1.26430	8.62E-09	NFκB
TNFSF9	1.00000	1.36E-03	-2.03650	8.17E-15	NFκB
TNFSF15	1.19150	2.94E-03	-2.26180	4.67E-18	None

BMP2	1.54300	3.27E-03	-1.69090	8.02E-03	NFκB
TGFBR1	0.70040	2.20E-02	-0.82610	2.84E-05	NFκB
IL12A	1.68170	3.07E-02	-1.53970	1.53E-02	NFκB
PRLR	2.91580	3.15E-02	-3.27440	4.52E-03	AP-1
IL15	0.85040	3.16E-02	-1.26610	1.07E-06	NFκB
IL23A	1.82120	5.59E-02	-1.58160	1.52E-02	NFκB/AP-1
IL2RG	0.95541	1.01E-01	-1.82390	5.10E-01	None
TNFRSF12A	0.71783	1.18E-01	-0.43630	6.51E-03	AP-1
TNFRSF14	0.46530	1.53E-01	-0.48970	2.73E-03	None
TNFRSF10B	0.52018	1.97E-01	-0.35370	4.89E-02	NFκB
BMPR1B	1.02127	1.98E-01	-2.11260	2.99E-04	None
HGF	2.08440	2.92E-01	-2.90270	1.53E-02	NFκB
PDGFC	0.42220	2.94E-01	-0.84640	1.00E-05	NFκB
IL22RA1	3.47750	3.63E-01	-5.93710	5.43E-03	NFκB
CCR4	2.87390	4.03E-01	-3.34307	3.91E-01	NA
CSF2	1.64173	4.61E-01	-0.17474	5.04E-01	NFκB
OSMR	0.40440	5.10E-01	-0.24603	3.82E-01	None
TNFSF10	1.37807	5.88E-01	-0.74565	3.64E-01	None
PDGFRB	0.42136	7.46E-01	-1.75040	7.60E-05	AP-1
TNFSF13B	3.28969	NA	-3.31250	3.42E-02	NFκB
TNFRSF18	2.87284	NA	-2.91772	1.48E-01	AP-1
IL7R	3.67340	NA	-3.50272	NA	NFκB/AP-1
CX3CR1	2.38491	NA	-2.44076	NA	NFκB
TNF	5.49810	NA	-5.56714	NA	NFκB
CXCL9	3.32350	NA	-3.39533	NA	NFκB
IFNAR2	0.34410	NA	-0.39382	9.84E-02	AP-1
INHBA	0.83100	NA	-3.20137	2.55E-01	None
CCL8	2.91000	NA	-2.98153	NA	None
CSF2RB	1.54048	NA	-2.04434	6.12E-02	None
Cell Adhesion Molecules (n=23)					
HLA-B	1.54750	1.24E-10	-2.12490	4.67E-29	NFκB
NRCAM	2.08430	1.99E-10	-3.42680	3.44E-08	None
CLDN14	2.72790	8.91E-10	-1.73390	1.61E-02	None
HLA-F	2.57600	2.25E-07	-4.58300	1.43E-14	NFκB
ICAM1	3.58140	4.18E-07	-3.17350	3.58E-04	NFκB
VCAM1	10.39070	6.70E-07	-7.44920	3.86E-04	NFκB
CNTNAP1	1.13470	8.81E-06	-0.87440	3.03E-07	None

ICOSLG	3.32720	1.44E-05	-3.15500	4.04E-03	None
CLDN1	2.09970	2.08E-05	-4.77710	1.22E-12	None
ITGAV	1.70150	6.11E-05	-1.20700	8.66E-03	None
HLA-C	0.85300	2.49E-04	-1.31420	9.92E-15	None
HLA-A	0.83990	3.40E-04	-0.81560	2.38E-06	NFκB
SDC4	0.91350	5.62E-04	-0.79390	6.91E-05	None
PDCD1LG2	0.98570	2.49E-03	-0.96010	1.02E-04	NFκB
SDC1	0.90460	1.09E-02	-1.18610	1.06E-06	None
SDC3	0.41120	4.08E-02	-1.86010	7.91E-51	None
CLDN23	1.91240	1.40E-01	-4.50220	1.21E-05	None
SELE	4.44980	1.87E-01	-9.34310	4.74E-05	NFκB
ITGB8	0.61910	2.80E-01	-2.01250	1.03E-10	NFκB
HLA-G	0.77070	3.23E-01	-1.45580	2.09E-03	None
MADCAM1	0.83220	7.39E-01	-0.84027	NA	None
HLA-DQA1	2.94940	NA	-3.01068	NA	None
CD6	1.94430	NA	-2.00757	NA	None

FDR: False Discovery Rate, NA: Not Available, TAK1-KO: TAK1 knockout, TNF: TNFα, WT: Wild-type.

799 **Table S2. Key Resources table**

REAGENT or RESOURCE	SOURCE	IDENTIFIER
Antibodies		
IκBα (L35A5) mouse mAb	Cell Signaling Technology	4814
Phospho-NFκB p65 (Ser536) (93H1) rabbit mAb	Cell Signaling Technology	3033
NFκB p65 (C22B4) rabbit mAb	Cell Signaling Technology	4764
Phospho-p44/42 MAPK (Erk1/2) (Thr202/Tyr204) rabbit pAb	Cell Signaling Technology	9101
p44/42 MAPK (Erk1/2) (137F5) rabbit mAb	Cell Signaling Technology	4695
Phospho-TAK1 (Ser412) rabbit pAb	Cell Signaling Technology	9339
TAK1 rabbit pAb	Cell Signaling Technology	4505
Phospho-SAPK/JNK (Thr183/Tyr185) (G9) mouse mAb	Cell Signaling Technology	9255
SAPK/JNK rabbit pAb	Cell Signaling Technology	9252
Phospho-p38 MAPK (Thr180/Tyr182) rabbit pAb	Cell Signaling Technology	9211
p38 MAPK (D13E1) XP® rabbit mAb	Cell Signaling Technology	8690
Actin (clone C4) mouse mAb	Merck Millipore	MAB1501
TAK1 rabbit pAb	Novus Biologicals	NBP1-87819
Human CD31 mouse mAb	DAKO	M0823
Iba1 rabbit pAb	FUJIFILM Wako Chemicals	019-19741
Isolectin GS-IB4 from Griffonia simplicifolia, Alexa Fluor™ 488 conjugate	Life Technologies Australia	I21411
Goat anti-mouse IgG HRP-conjugated secondary Ab	Merck Millipore	12-349
Goat anti-rabbit Alexa Fluor 488 plus secondary Ab	Invitrogen	A32731

Goat anti-mouse Alexa Fluor 594 plus secondary Ab	Invitrogen	A32742
NucBlue™ Reagent (Hoechst 33342)	Life Technologies Australia	R37605
Chemicals		
5Z-7-oxozeaenol	Tocris Bioscience	3604/1
3-(4,5-dimethylthiazol-2-yl)-2,5-diphenyl-2H-tetrazolium bromide (MTT)	Sigma-Aldrich	M2128
DMSO	Sigma-Aldrich	D8418
Sodium citrate dihydrate	Sigma-Aldrich	W302600
Triton X100	Sigma-Aldrich	T8787
Ampicillin	Sigma-Aldrich	A0166
Polybrene	Sigma-Aldrich	H9268
Puromycin	Sigma-Aldrich	P8833
Agarose	Sigma-Aldrich	A6361
Critical Commercial Assays		
Pierce™ BCA assay kit	Life Technologies Australia	23227
Amersham ECL Prime Western Blotting Detection Kit	GE Healthcare	RPN2232
Q5 Hot Start High-Fidelity 2X Master Mix	New England Biolabs	M0494
High-capacity cDNA reverse transcription Kit	Life Technologies Australia	4368814
TaqMan™ Fast Advanced Master Mix	Life Technologies Australia	4444553
Quick-RNA MiniPrep kit	Zymo Research	R1055
Agencourt CleanSeq Kit	Beckman Coulter	A29151
ZymoPURE Plasmid Miniprep Kit	Zymo Research	D4210
Quick-DNA Microprep Kit	Zymo Research	D3021
Experimental Models: Cell Lines		
Telomerase-immortalized human microvascular endothelial cells (TIMEs)	American Type Culture Collection	ATCC® CRL-4025™
Human retinal microvascular endothelial cells (HRMECs)	Cell Systems	ACBRI 181 V
Human embryonic kidney 293FT	Life Technologies Australia	R70007
Experimental Models: Organisms/Strains		

Sprague-Dawley rat and C57BL/6 mouse	St Vincent's Hospital	004/16
Brown Norway rat	University of Melbourne	13-044UM
Sprague-Dawley rat	University of Tasmania	A0017311
Oligonucleotides		
TAK1 sgRNA#1 Forward	Integrated DNA Technologies	CACCGTAGACCAACAACGAGTCATC
TAK1 sgRNA#1 Reverse	Integrated DNA Technologies	AAACGATGACTCGTTGTTGGTCTAC
TAK1 sgRNA#2 Forward	Integrated DNA Technologies	CACCGGAGTTGTTTGCAAAGCTAAG
TAK1 sgRNA#2 Reverse	Integrated DNA Technologies	AAACCTTAGCTTTGCAAACAACTCC
TAK1 sgRNA#3 Forward	Integrated DNA Technologies	CACCGGAGGAAAGCGTTTATTGTAG
TAK1 sgRNA#3 Reverse	Integrated DNA Technologies	AAACCTACAATAAACGCTTTCCTCC
TAK1 sgRNA cassettes PCR Forward	Integrated DNA Technologies	TGAGTATTACGGCATGTGAGGGC
TAK1 sgRNA cassettes PCR Reverse	Integrated DNA Technologies	TCAATGTATCTTATCATGTCTGCTCGA
Human MAP3K7 siRNA (Smartpool)	Dharmacon	n/a
Human Control siRNA	Dharmacon	n/a
qPCR Probes		
Rat Map3k7 TaqMan probe	Applied Biosystems	Rn01437015_m1
Rat Tnf alpha TaqMan probe	Applied Biosystems	Rn01525859_g1
Rat Vegf-a TaqMan probe	Applied Biosystems	Rn01511602_m1
Rat Icam-1 TaqMan probe	Applied Biosystems	Rn00564227
Rat beta actin TaqMan probe	Applied Biosystems	Rn00821065_g1
Human MAP3K7 TaqMan probe	Applied Biosystems	Hs00177373_m1
Human VEGF-A TaqMan probe	Applied Biosystems	Hs00900055_m1
Human ICAM-1 TaqMan probe	Applied Biosystems	Hs00164932_m1
Human VCAM-1 TaqMan probe	Applied Biosystems	Hs01003372_m1
Human CXCL8 TaqMan probe	Applied Biosystems	Hs00174103_m1
Human GAPDH TaqMan probe	Applied Biosystems	Hs99999905_m1
Software and Algorithms		

Image Pro Plus	Media Cybernetics	n/a
Incucyte® Live-Cell Imaging and Analysis System	Sartorius	n/a
ImageJ version 1.48	Schneider et al., 2012 https://imagej.nih.gov/ij	n/a
Adobe Photoshop	Adobe. Connor et al., 2009	n/a
AngioTool Software	NIH. Zudaire et al., 2011	n/a
FIJI software	https://fiji.sc/	n/a
Prism 7	GraphPad Software	n/a
R (v4.0.2)	Bioconductor	n/a
Trimgalore (0.4.4)	Babraham Institute	n/a
STAR (2.5.3)	Alexander Dobin	n/a
FeatureCounts (subread 1.6.4)	Liao Y, Smyth GK and Shi W., 2014	n/a
Other		
Pierce RIPA buffer	Life Technologies Australia	89900
Protease inhibitor cocktail	Roche Diagnostics	11697498001
Recombinant Human TNF-α protein	Gibco™	PHC3015
Bolt™ 4-12% Bis-Tris Plus Gel	Invitrogen	NW04120BOX
Immun-Blot® PVDF Membrane	Bio-Rad Laboratories	1620177
Human VEGF protein	R&D Systems	293-VE-010
Matrigel™ Basement Membrane Matrix	Corning	356234
Normal donkey serum	Sigma-Aldrich	D9663
PBS	Gibco™	14190-144
Antibody Diluent	DAKO	S0809
Fluorescence Mounting Medium	DAKO	S3023
BsmBI	New England Biolabs	R0580S
lentiCRISPRv2 plasmid	Addgene	52961
NEB Stable Competent E. coli cells	New England Biolabs	C3040I
pCMV-dR8.91 (plasmid)	RNAiCore; Academia Sinica, Taipei, Taiwan	n/a
pMD2.G (plamid)	Addgene	12259

Lipofectamine 2000	Life Technologies Australia	11668019
0.45µm PDVF syringe filter	Merck Millipore	SLHV033RS
5x PEG-it	System Biosciences	LV810A-1
Opti-MEM	Life Technologies Australia	31985070
EBMTM Plus Basal Medium supplied with EGMTM Plus SingleQuotsTM supplements	Lonza	CC-5035
MycoAlert™ Mycoplasma Detection Kit	Lonza	LT07
Dulbecco's modified Eagle's medium	Life Technologies Australia	11965092
Glutamine	Life Technologies Australia	2503008
Penicillin-streptomycin	Life Technologies Australia	15070063
Fetal bovine serum	Sigma-Aldrich	F9423
TrypLE Express Enzyme (1X)	Life Technologies Australia	12605028

800

801

802 **SUPPLEMENTARY METHODS**

803 **Generation of TAK1-KO TIME cell line**

804 Three sgRNAs targeting the exonic regions of the human TAK1 gene (**Table S2**) were designed on
805 CHOPCHOP (https://chopchop.cbu.uib.no). The annealed oligos ordered from the Integrated DNA
806 Technologies (IDT; Coralville, Iowa, USA) representing the various sgRNAs were cloned into the
807 BsmBI sites (R0580S; New England Biolabs) of the lentiCRISPRv2 plasmid (52961; Addgene). The
808 plasmid was validated by Sanger sequencing with 3500 Series Genetic Analyzers (Thermo Fisher
809 Scientific; Waltham, MA). HEK293FT cells (R70007; Life Technologies) were plated at 1×10^7 cells
810 per T75 flask one day prior to transfection. Lentivirus was made by co-transfecting lentiCRISPRv2
811 (15µg), pCMV Δ8.91 (15µg) and pMDG plasmids (1.5µg) (RNAiCore; Academia Sinica, Taipei,
812 Taiwan) in HEK293FT cells using Lipofectamine 2000 (11668019; Life Technologies). Media was
813 changed 5 hours post transfection. The virus-containing media was harvested and filtered through a
814 0.45 µm PDVF syringe filter (SLHV033RS; Merck Millipore) to remove cell debris 48 hours post
815 transfection. Lentivirus aliquots were precipitated by 5x PEG-it (LV810A-1; System Biosciences) at
816 4°C overnight and centrifugated at 1500g at 4°C for 30 minutes. After discarding the supernatant, the
817 lentivirus were resuspend within opti-MEM ready for use. Wild type TIME cells (7.5×10^5) were plated
818 at T75 flask before transduction. When grow to 50% confluence, cells were transduced by TAK1
819 sgRNA lentiCRISPRv2 lentivirus with polybrene (8µg/mL) (H9268; Sigma-Aldrich) for 72 hours.
820 Medium containing 0.5 µg/mL puromycin (P8833; Sigma-Aldrich) was then replaced for another 72
821 hours to select stable clones which were subsequently cultured as the stable TAK1 KO cell lines.
822

823 **Single colony selection of TAK1-KO cell line**

824 Once the selected TAK1 KO cell lines reached 80% confluence, cells were trypsinized from the stable
825 cell pool using TrypLE Express Enzyme (1X) (12605028; Life Technologies) to break up any clumps
826 into individual cells. TAK1-KO cells were then diluted to a density of 5 cells/mL and resuspended
827 with 100 ul placed in each well in 96-well plate. After expanding for 7-14 days, colonies of single cells
828 were subsequently cultured as the single colony selected TAK1-KO cell line in culture dishes by
829 trypsinization.
830

831 **Identification of TAK1 indels in TAK1-KO line**

832 Genomic DNA was isolated from wild type and TAK1-KO TIME cell lines using Quick-DNA
833 Microprep Kit (D3021; Zymo Research) according to the manual. Extracted genomic DNA was used
834 as a PCR template to amplify the target of the TAK1 sgRNA using sequence specific primers (**Table**
835 **S2**). Briefly, PCR reactions were made up to 25 µL comprising 12.5 µL Q5 Hot Start High-Fidelity

836 2X Master Mix (M0494; New England Biolabs), 1.25 µL of forward and reverse primers and the
837 diluted gDNA, under thermocycling conditions of 98°C initial denaturation for 30 seconds, and 30
838 cycles of 98°C denaturation for 10 seconds, 65°C annealing for 30 seconds, and 72°C extension for 30
839 seconds with a 72°C final extension for 2 minutes. The PCR amplification product was validated using
840 electrophoresis using 1% agarose gel (A6361; Sigma-Aldrich). The gDNA was then cleaned by using
841 a Quick-DNA Microprep Kit (D3021; Zymo Research). Following the first-round of PCR
842 amplification, a second round of sequencing PCR was performed. The second-round PCR products
843 were subsequently purified using Agencourt CleanSeq Kit (A29151; Beckman Coulter). The PCR
844 samples were denatured at 98°C for 5 minutes and sequenced by Sanger sequencing.
845
846 **Electroretinography (ERG) in rat**
847 Rats were dark-adapted overnight prior to the ERG assessment under fully dark-adapted conditions.
848 Details for functional assessment are as previously described (58). Briefly, a pair of custom-made
849 chloride silver active and ring-shaped reference electrodes (99.9%, A&E Metal Merchants, Sydney,
850 NSW, AU), connected to platinum leads (F-E-30, Grass Telefactor, West Warwick, RI), was place on
851 the central cornea and around the sclera, respectively. A stainless-steel needle electrode (F-E2-30,
852 Grass Telefactor) was inserted subcutaneously into the tail of the animal to act as the ground.
853 Measurements were recorded simultaneously for both eyes. ERG analysis was undertaken as
854 previously described to return measures for three major waveforms, which are known to reflects the
855 function of key retinal cells, specifically photoreceptors (a-wave), bipolar cells (b-wave), and ganglion
856 cells (scotopic threshold response, STR).
857
858 **Spectral-domain optical coherence tomography (OCT) in rat**
859 Following ERG measurement, rat eyes were imaged using Envisu R2200 VHR spectral domain-OCT
860 (Bioptigen, Inc., Morrisville, NC, USA). Volume scans consisting of 1000 A-scans per 100 B-scans
861 (100 horizontal B-scans evenly spaced in the 1.4 mm vertical dimension) centered on the optic nerve
862 head (ONH; 1.4 × 1.4 × 1.57 mm) were obtained from both eyes. Four B-scans that crossed the ONH
863 were analyzed using FIJI software (https://fiji.sc/). In each B-scan the inner limiting membrane, retinal
864 nerve fiber layer, inner plexiform layer and Bruch's membrane were manually segmented by a masked
865 observer as previously described (58). Total retinal thickness was measured from the inner limiting to
866 Bruch's membrane. Retinal nerve fiber layer thickness was measured from the inner limiting
867 membrane to the inner aspect of the inner plexiform layer. Outer retinal thickness was measured from
868 Bruch's membrane to the outer plexiform layer.

869 **SUPPLEMENTARY FIGURES**
870
871

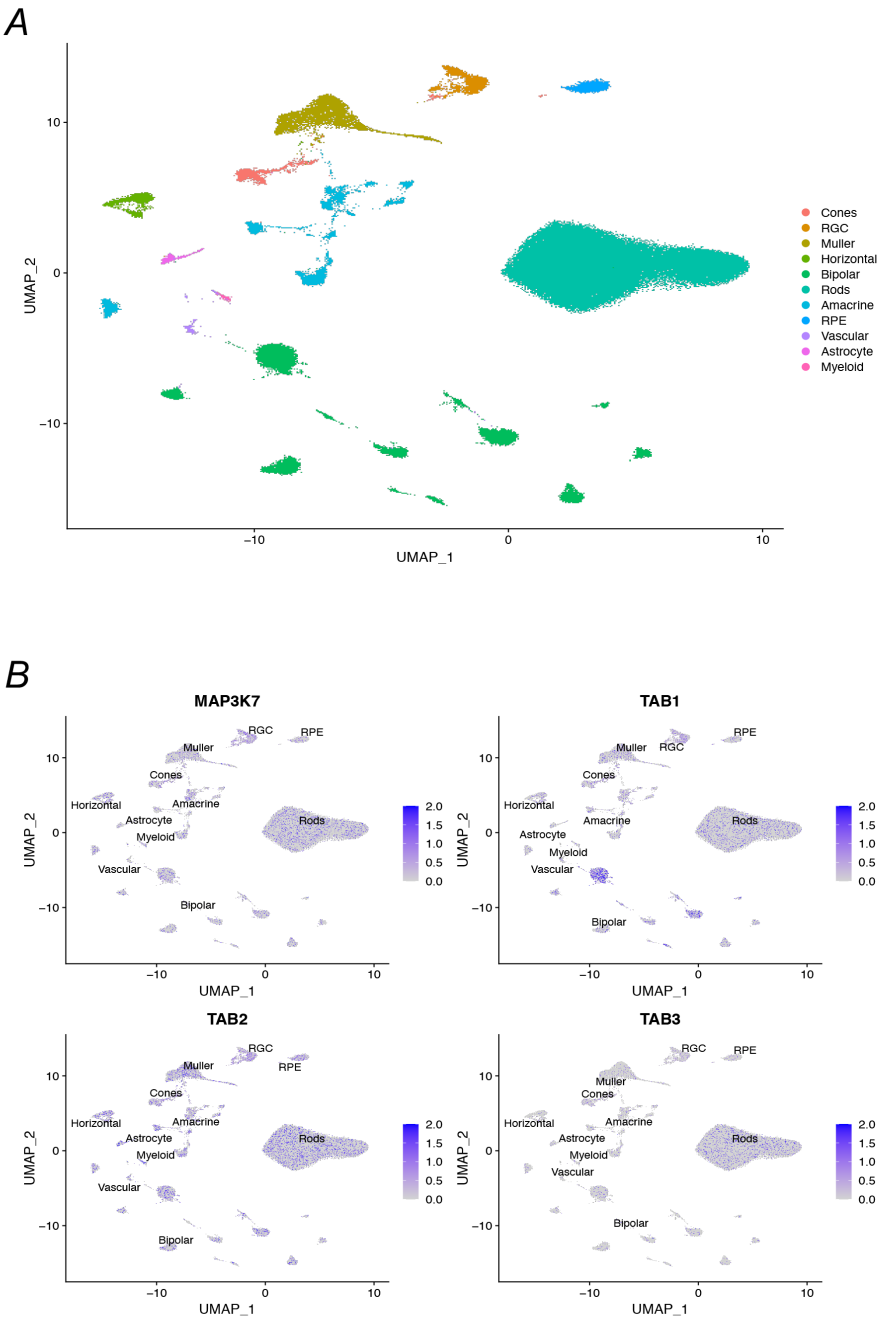

872
873 **Fig. S1** Uniform Manifold Approximation and Projection (UMAP) clustering of the integrated datasets
874 from snRNA-seq data (A) representing the expressions of TAK1 (MAP3K7) and TAK1-associated
875 proteins (TAB1-3) in identified retinal and non-retinal cellular clusters (B).
876

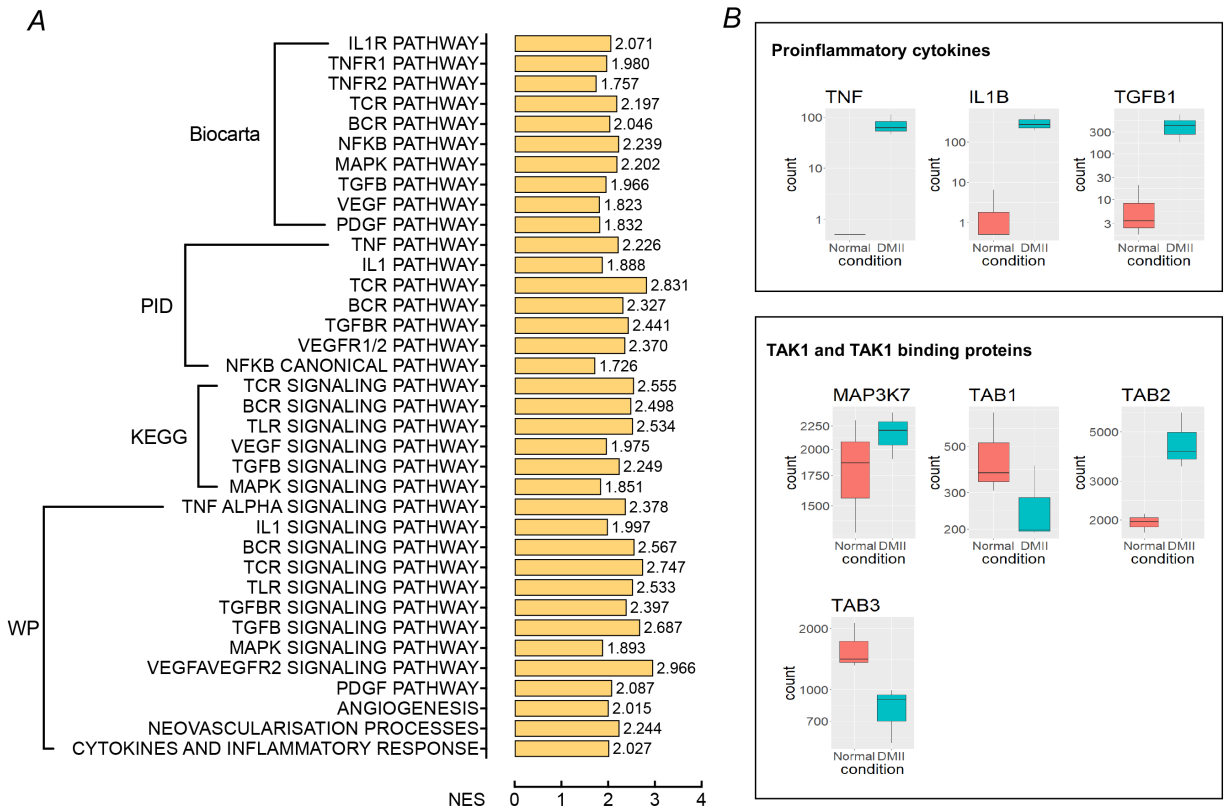

Fig. S2 (A) Gene set enrichment analysis (GSEA) revealed positive enrichment of TAK1 upstream pathways in the retinae from patients with retinal neovascularization due to proliferative diabetic retinopathy. Gene set database includes Biocarta, Pathway Interaction Database (PID), Kyoto Encyclopedia of Genes and Genomes (KEGG) and WikiPathways (WP). (B) Readcounts of selected genes related to TAK1 in the retinae from normal control and patients with retinal neovascularization due to diabetic retinopathy. False discovery rate (FDR) was set at a q value <0.05.

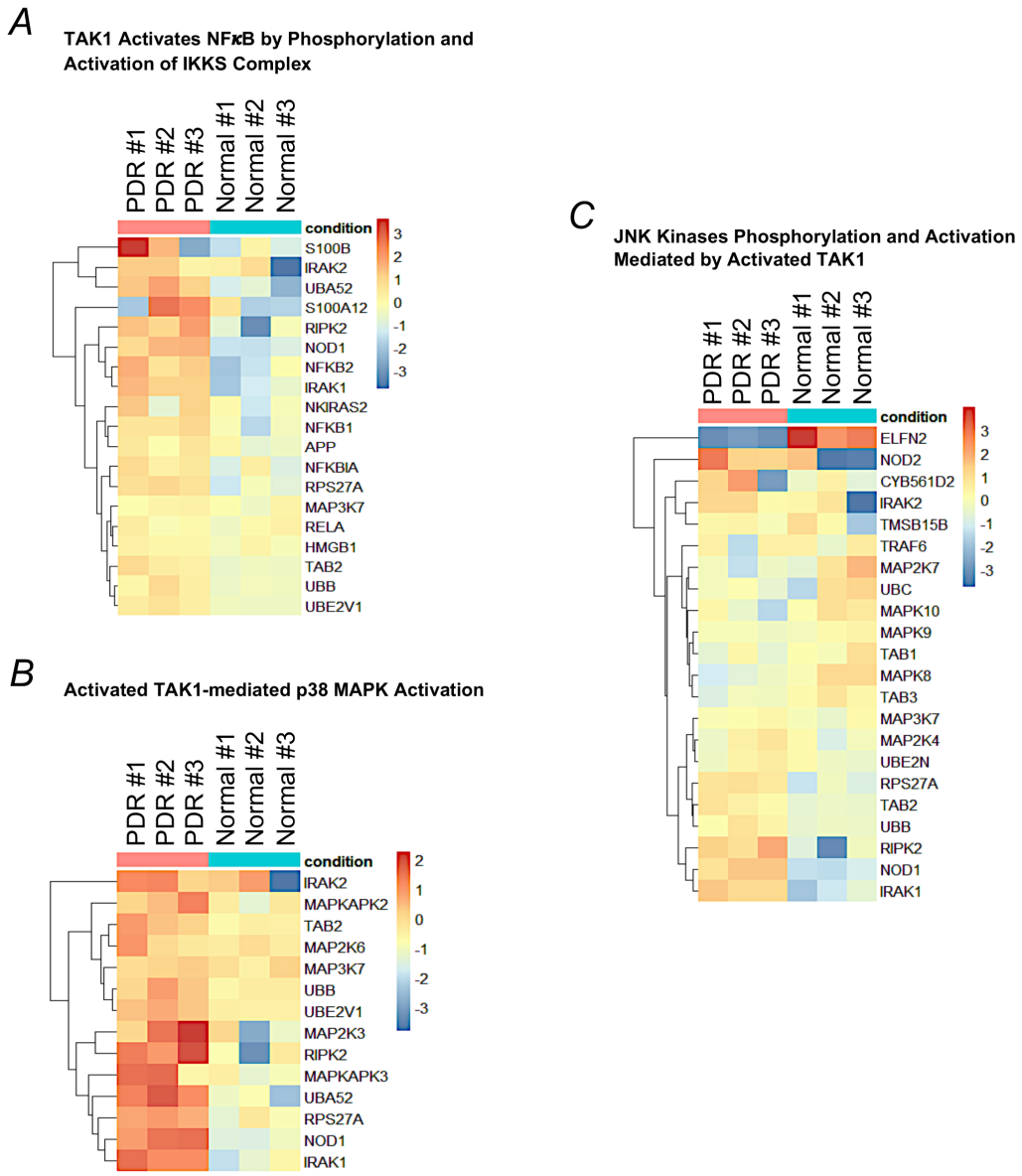

Fig. S3 Heat maps generated from unsupervised clustering of genes from Reactome Pathway Database of (A) "TAK1 Activates NFκB by Phosphorylation and Activation of IKKS Complex", (B) "Activated TAK1-mediated p38 MAPK Activation, and (C) "JNK kinases phosphorylation and activation mediated by activated TAK1". False discovery rate (FDR) was set at a q value <0.05.

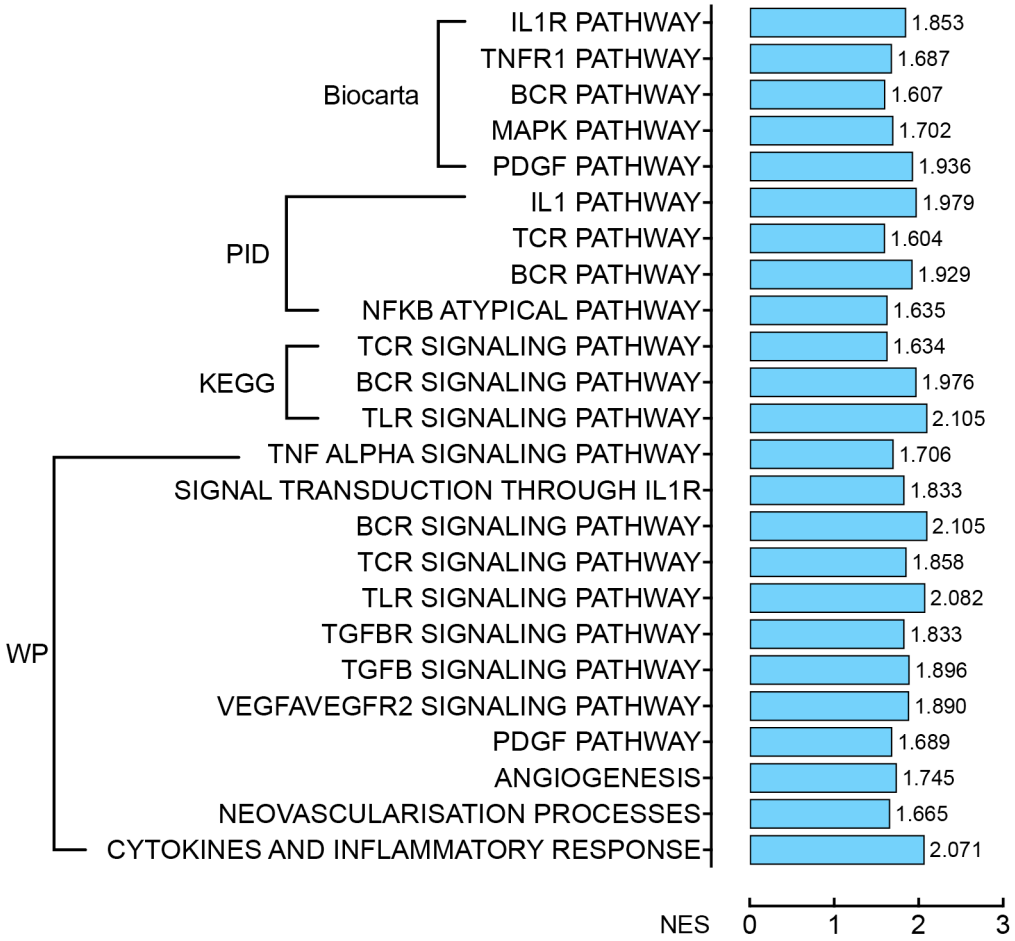

Fig. S4 Gene-set enrichment analysis from multiple databases indicated the positive impact of TAK1 upstream pathways in rat OIR retinas. Genome-wide transcriptional analysis of rat OIR retina samples indicated the differential gene expression associated with positive impact in TAK1 upstream pathways. Biocarta, Pathway Interaction Database (PID), Kyoto Encyclopedia of Genes and Genomes (KEGG), and WikiPathways (WP) gene sets were used in GSEA. False discovery rate (FDR) was set at a q value <0.05.

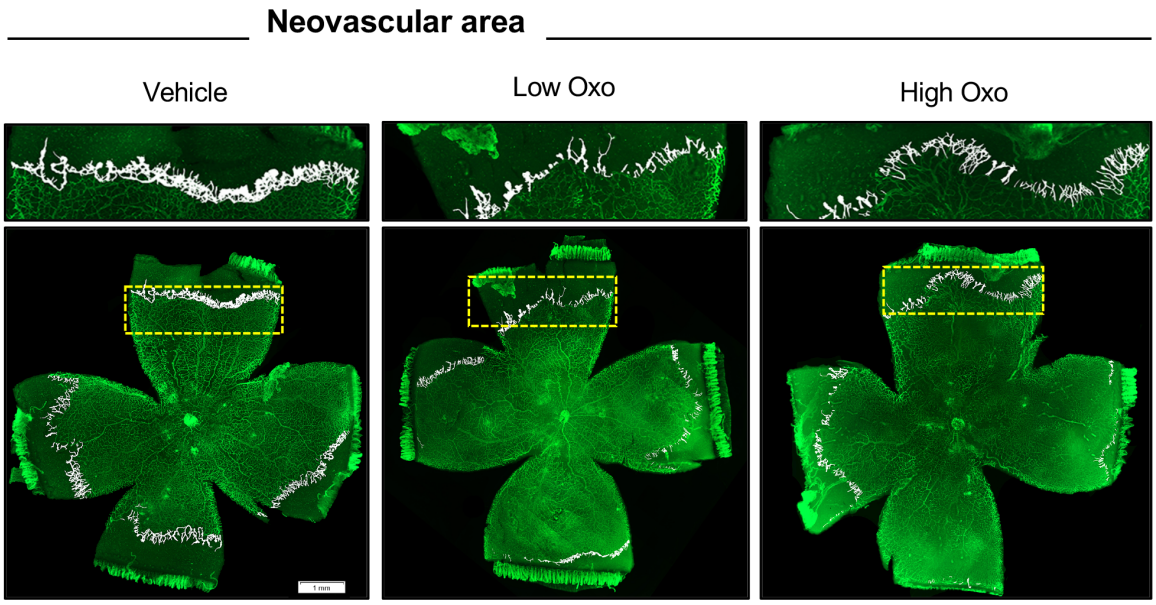

Fig. S5 Uncropped retinal flat mounts. The region indicated by the dashed line was used to show retinal neovascularization (highlighted in white) in Fig. 3B. Oxo: 5Z-7-oxozeaenol. Scale bar: 1 mm.

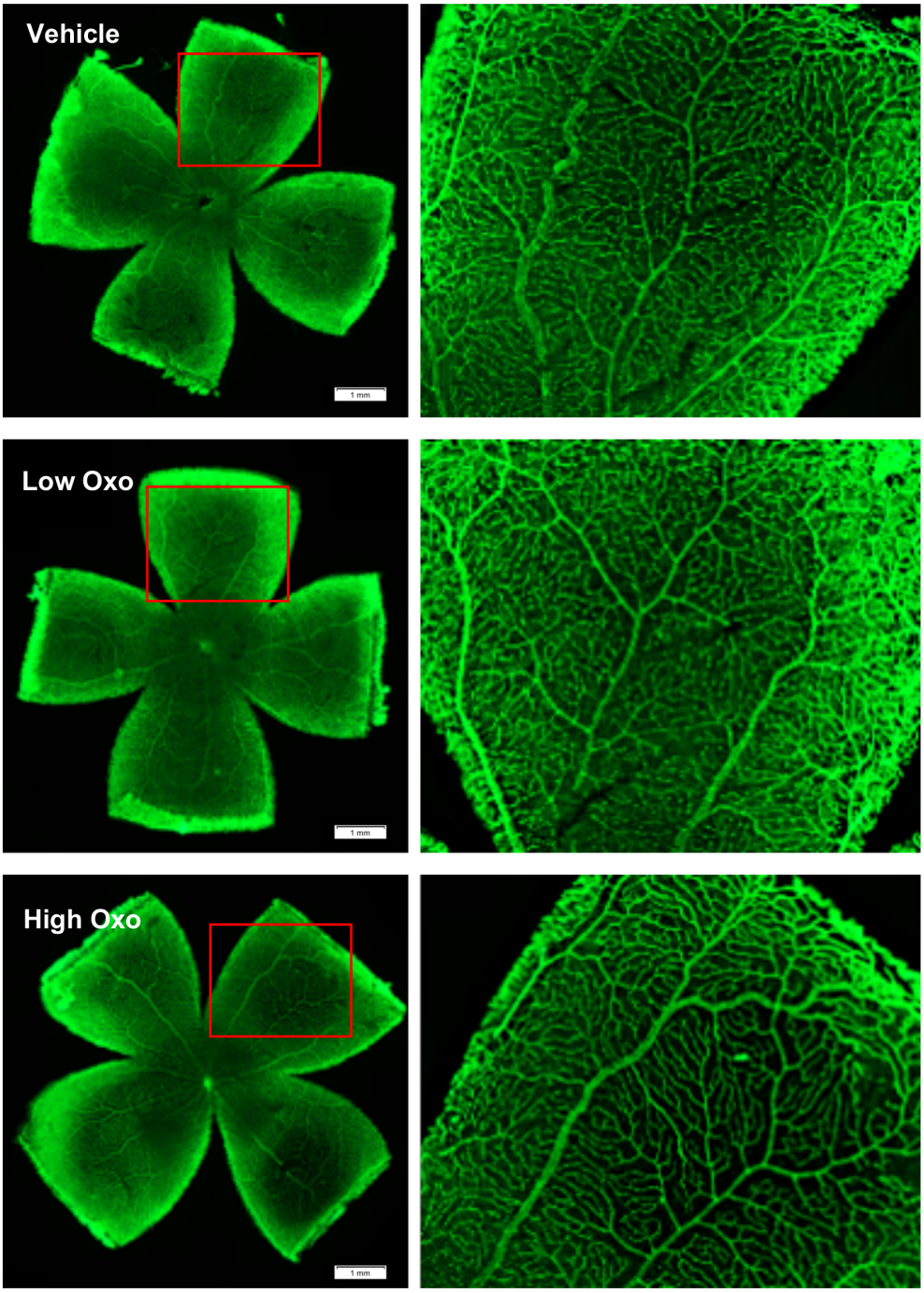

Fig. S6 Inhibition of TAK1 did not cause retinal vessel remodeling. Retinal flat mount was labelled with IB4 28 days after a single intravitreal injection of vehicle, low (18 ng) or high (90 ng) dose of 5Z-7-oxozeaenol (Oxo) in normoxic rats to examine drug effects on normal retinal vasculature. Scale bar: 1 mm.

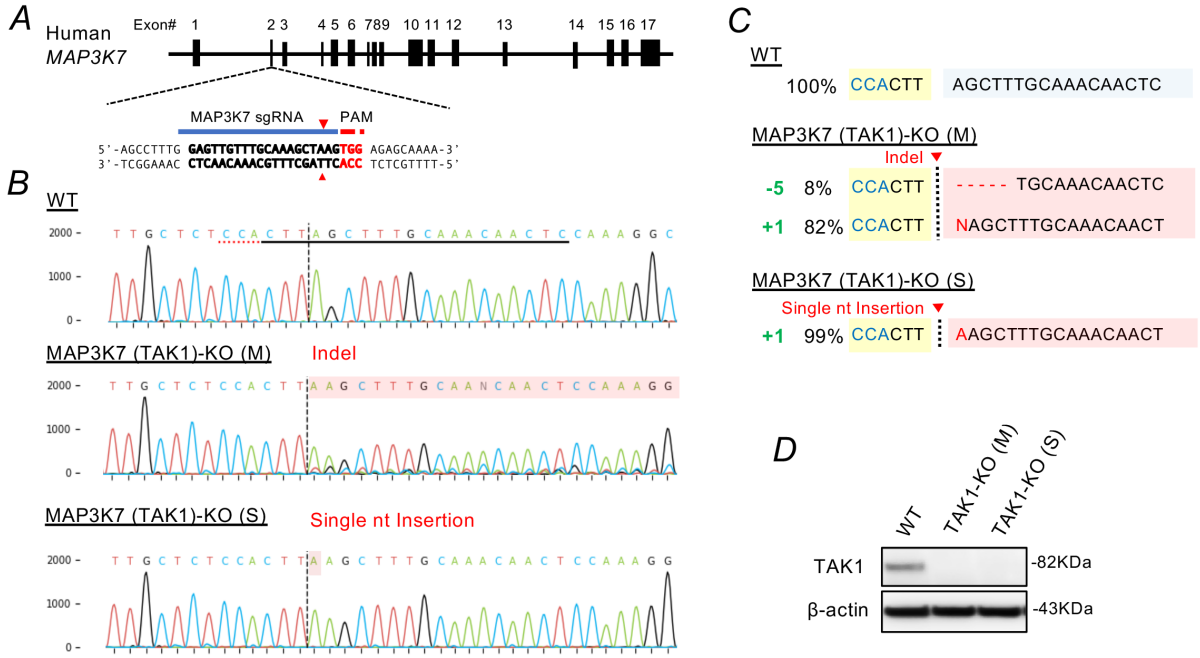

Fig. S7 Generation of CRISPR/Cas9-mediated MAP3K7 knockout (TAK1-KO) in human endothelial cells. (A) Genome of TAK1 (MAP3K7). A sgRNA was designed to target exon 2 of the TAK1 gene. (B) As compared with wild-type (WT) TIMEs, genomic DNA sequences revealed a heterogeneous MAP3K7-KO (M) and a single homogenous MAP3K7-KO (S) TIMEs were established after CRISPR/Cas9 gene editing. (C) Sanger sequencing confirmed that MAP3K7-KO (M) TIMEs had mixed indel profiles, and MAP3K7-KO (S) TIMEs was a single nucleotide insertion, which created as premature Stop Condon in TAK1 exon 2 region. (D) Western blot characterization of TAK1 knockout in MAP3K7-KO (M) and MAP3K7-KO (S) TIMEs.

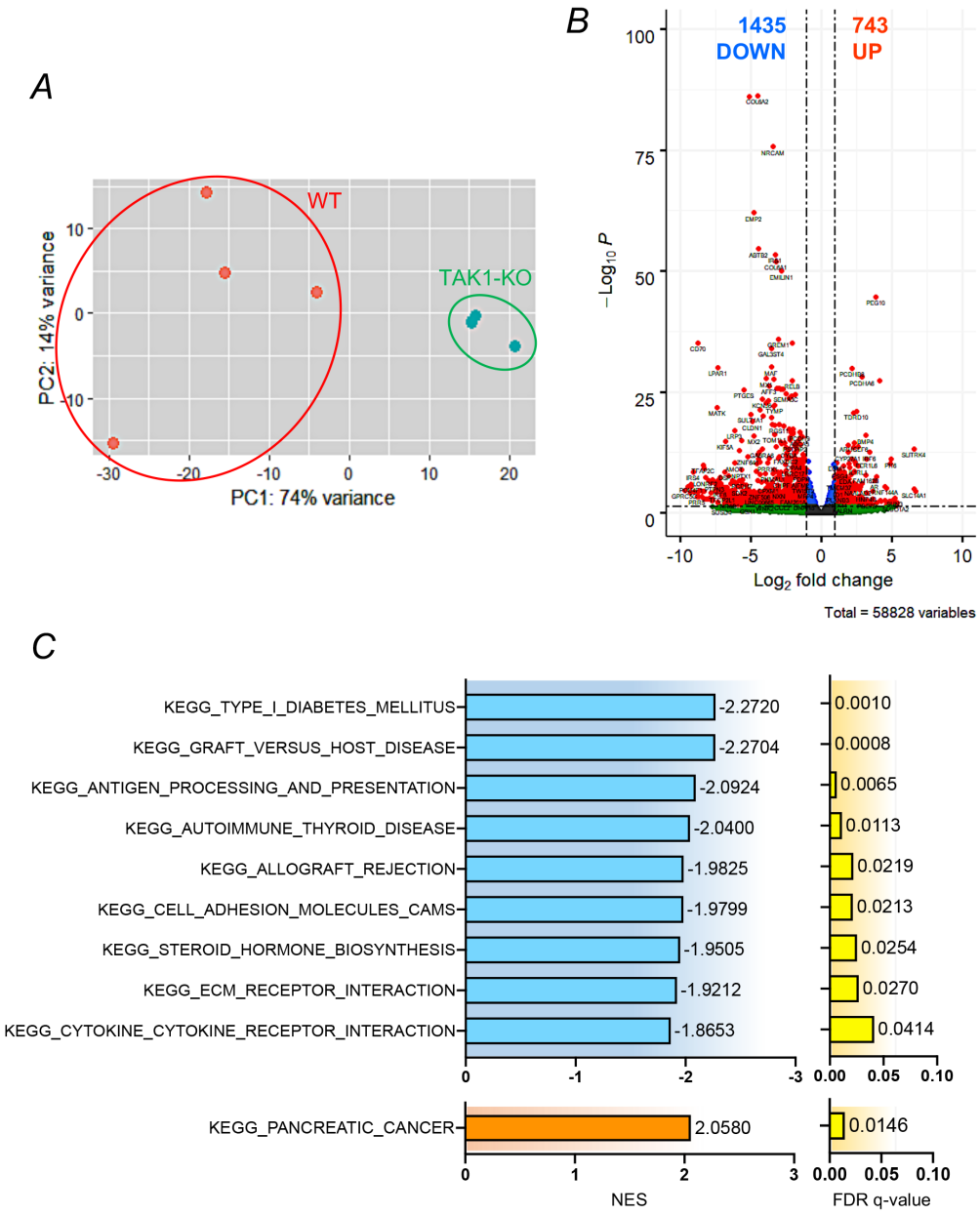

Fig. S8 (A) Principal components analysis of RNA-seq data of wild type cells, wild-type (WT) cells and TAK1 knockout (TAK1-KO) TIMEs. Each dot represents an experimental replicate. (A) Volcano plots showing genes that were significantly different between WT and TAK1-KO TIMEs. Red dots refer to genes showing a log2|fold change| > 1 and FDR < 0.05. Labels indicate the significantly up-regulated genes in each data set. (C) Gene set enrichment analysis (GSEA) revealed the top 10 Kyoto Encyclopedia of Genes and Genomes (KEGG) pathways that were positively or negatively enriched in TAK1-KO TIMEs. False discovery rate (FDR) was set at a q value <0.05.

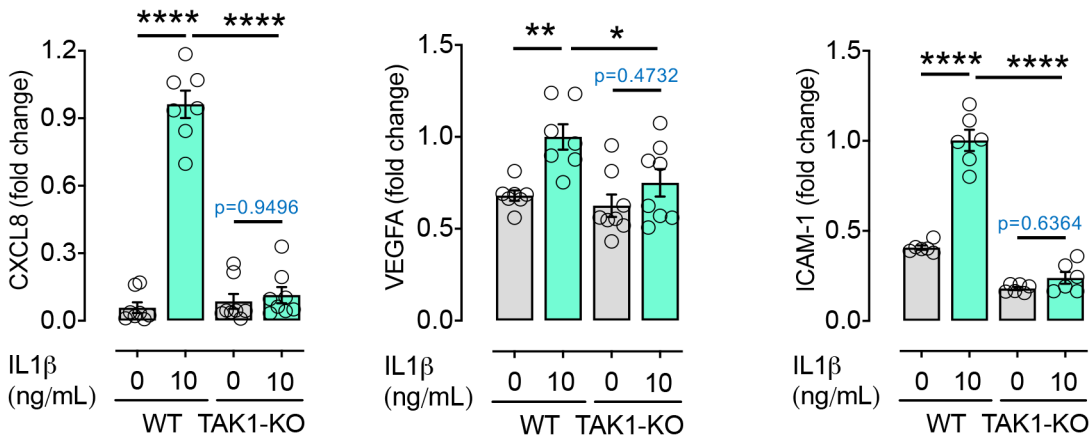

Fig. S9 TAK1 deletion reduced the expression of *TAK1, ICAM-1, CXCL8 and VEGF* genes in human microvascular endothelial cells. qPCR results revealed that TAK1 deletion suppressed the expression of selected cytokines (*CXCL8* and *VEGFA)* and adhesion molecules (*ICAM-1)* in TIMEs stimulated with IL1β for 24 hours (n = 4; technical duplicate from each biological repeat was shown as separated dot plot). Group data are shown as means ± SEM. Statistical analysis was undertaken with one-way ANOVA and Tukey's multiple comparison test; $*P < 0.05$, $**P < 0.01$, $***P < 0.001$, $****P < 0.0001$.

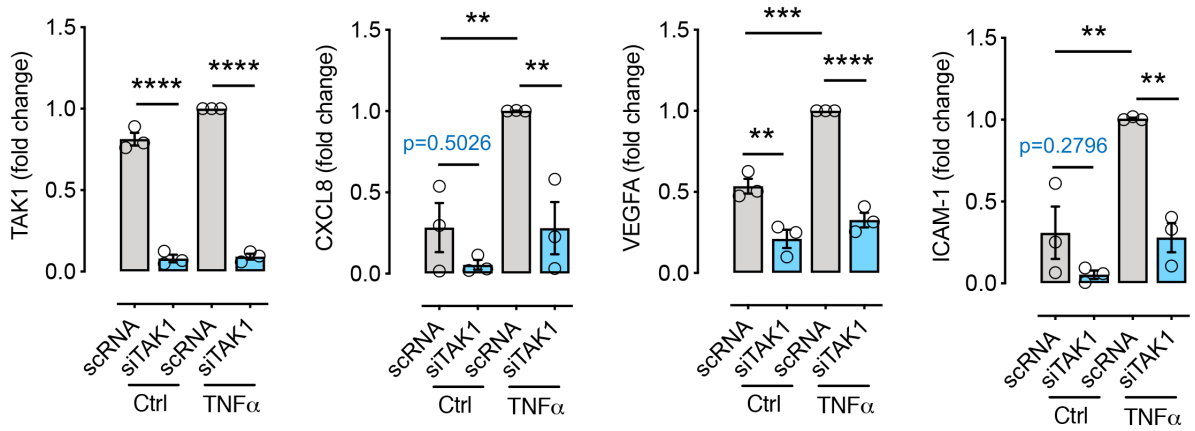

Fig. S10 TAK1 knockdown by siRNA inhibited the expression of *TAK1, ICAM-1, CXCL8 and VEGF* genes in human primary retinal microvascular endothelial cells (HRMECs). qPCR results revealed that TAK1 knockdown by siRNA targeting TAK1 (siTAK1) suppressed the expression of selected cytokines (*CXCL8* and *VEGFA)* and adhesion molecules (*ICAM-1)* in HRMECs stimulated with TNFα for 24 hours (n = 3). Group data are shown as means ± SEM. Statistical analysis was undertaken with one-way ANOVA and Tukey's multiple comparison test; $^{**}P < 0.01$, $^{***}P < 0.001$, $^{****}P < 0.0001$.

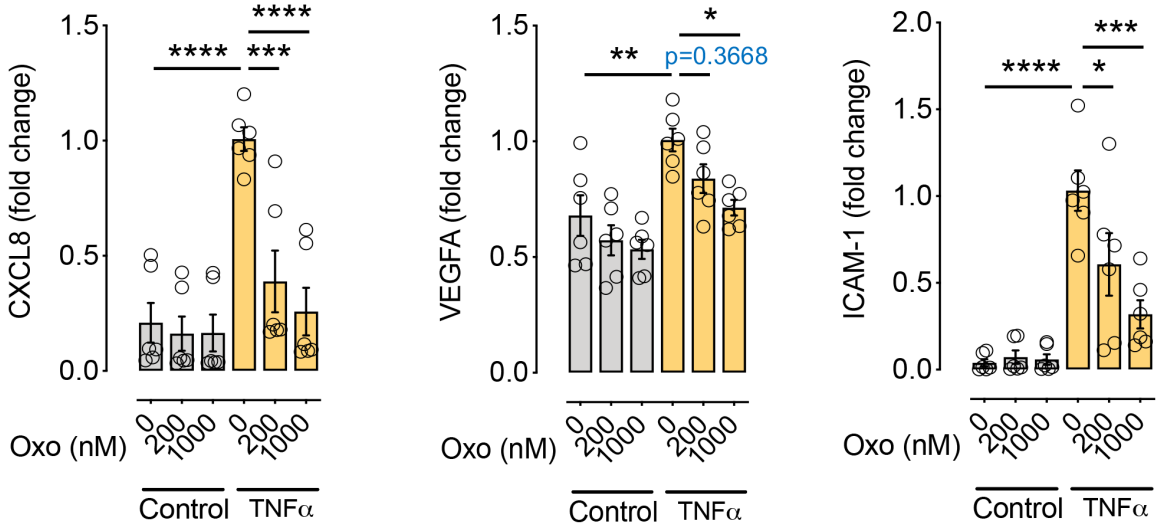

Fig. S11 TAK1 inhibition by 5Z-7-oxozeaenol inhibited the expression of *TAK1, ICAM-1, CXCL8 and VEGF* genes in primary human retinal microvascular endothelial cells (HRMECs). qPCR results revealed that pharmacological inhibition of TAK1 by 5Z-7-oxozeaenol (Oxo) suppressed *ICAM-1*, *PTGS2*, *CXCL8* and *VEGFA* in HRMECs stimulated with TNFα in a dose-dependent manner (n = 3; technical duplicate from each biological repeat was shown as separated dot plot). Group data are shown as means ± SEM. Statistical analysis was undertaken with one-way ANOVA and Tukey's multiple comparison test; *$P < 0.05$, **$P < 0.01$, ***$P < 0.001$, ****$P < 0.0001$.

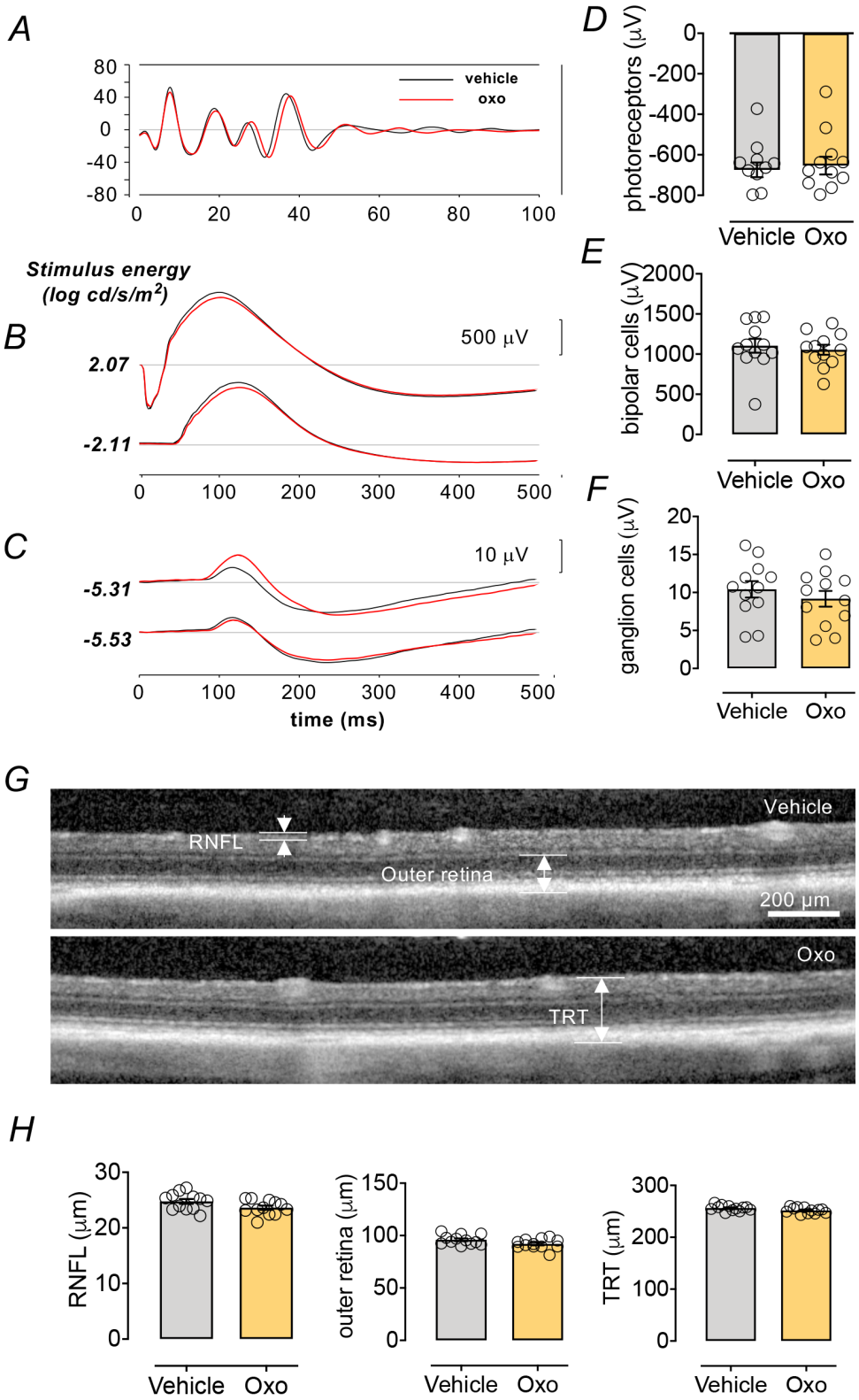

Fig. S12 Effect of 5Z-7-oxozeaenol (Oxo) on *in vivo* retinal structure and function. ERG and OCT were performed 28 days after intravitreal injection of 5Z-7-oxozeaenol (90 ng) in normoxia Brown Norway rats. No difference was observed between the vehicle- (black traces) and 5Z-7-oxozeaenol-injected (red traces) eyes in terms of the average amacrine cell oscillatory potentials (A)

1034 photoreceptoral and bipolar cell responses (B) or ganglion cell responses (C) in 5Z-7-oxozeaenol-
1035 injected eyes (n = 11, red traces) and corresponding vehicle-injected eyes (n = 12, black traces). Group
1036 average (± SEM) photoreceptor (D. $P = 0.71$) bipolar cell (E. $P = 0.63$) and ganglion cell (F, $P = 0.41$).
1037 Response amplitude were not different between 5Z-7-oxozeaenol-injected eyes and corresponding
1038 vehicle-injected eyes. (G) Representative OCT images from a 5Z-7-oxozeaenol- and vehicle-injected
1039 eye. (H) Total retinal thickness (TRT), outer retina, and retinal nerve fiber layer (RNFL) thickness
1040 were not different between groups ($P = 0.0639$ of TRT, $P=0.0502$ of outer retina, $P = 0.064$ of RNFL).
1041 All data are shown expressed as means ± SEM. Statistical analysis was undertaken with two-tailed
1042 Student's *t*-test.
1043